Early View

Original research article

Inhaled Seralutinib Exhibits Potent Efficacy in Models of Pulmonary Arterial Hypertension

Anna Galkin, Ravikumar Sitapara, Bryan Clemons, Eduardo Garcia, Michael Kennedy, David Guimond, Laura L. Carter, Ashley Douthitt, Robin Osterhout, Aneta Gandjeva, Deborah Slee, Luisa Salter-Cid, Rubin M. Tuder, Lawrence S. Zisman

Inhaled Seralutinib Exhibits Potent Efficacy in Models of Pulmonary Arterial Hypertension

Anna Galkin[1*], Ravikumar Sitapara[1,2*], Bryan Clemons[1], Eduardo Garcia[1], Michael Kennedy[1], David Guimond[1], Laura L. Carter[1], Ashley Douthitt[1], Robin Osterhout[1], Aneta Gandjeva[4] Deborah Slee[1], Luisa Salter-Cid[1], Rubin M. Tuder[4], Lawrence S. Zisman[1,3]

[1]Gossamer Bio, Inc., San Diego, CA; [2]The Rensselaer Center for Translational Research Inc; Rensselaer, NY; [3]Pulmokine Inc.; Troy, NY, [4]University of Colorado School of Medicine, Aurora, CO

Corresponding Author:

Lawrence S. Zisman, MD

Gossamer Bio, Inc.

3013 Science Park Road

San Diego, CA 92121

Email: lzisman@gossamerbio.com

Phone: 858-684-1730

Short title: Seralutinib in pulmonary arterial hypertension

Total number of manuscript pages: 31; Online supplement: 27 pages

Total number of figures: 8 (plus 8 supplemental figures/3 tables)

Word count for body of the text: 3297

Type of contribution: original article

Key words: kinase inhibitor, PDGFR, CSF1R, c-KIT

Author Contributions

*Dr. Anna Galkin and Dr. Ravikumar Sitapara contributed equally as first author contributors in the generation and interpretation of data and development of content for this manuscript.

Substantial contributions to the conception or design of the work; or the acquisition, analysis, or interpretation of data for the work: Anna Galkin, Ravi Sitapara, Bryan Clemons, Eduardo Garcia, Michael Kennedy, David Guimond, Laura Carter, Ashley Douthitt, Robin Osterhout, Aneta Gandjeva, Debbie Slee, Luisa Salter-Cid, Rubin M. Tuder, Lawrence S. Zisman

Drafting the work or revising it critically for important intellectual content: Anna Galkin, Ravi Sitapara, Bryan Clemons, Eduardo Garcia, Michael Kennedy, David Guimond, Laura Carter, Ashley Douthitt, Robin Osterhout, Aneta Gandjeva, Debbie Slee, Luisa Salter-Cid, Rubin M. Tuder, Lawrence S. Zisman

Final approval of the version submitted for publication: Anna Galkin, Ravi Sitapara, Bryan Clemons, Eduardo Garcia, Michael Kennedy, David Guimond, Laura Carter, Ashley Douthitt, Robin Osterhout, Aneta Gandjeva, Debbie Slee, Luisa Salter-Cid, Rubin M. Tuder, Lawrence S. Zisman

Agreement to be accountable for all aspects of the work in ensuring that questions related to the accuracy or integrity of any part of the work are appropriately investigated and resolved: Anna Galkin, Ravi Sitapara, Bryan Clemons, Eduardo Garcia, Michael Kennedy, David Guimond, Laura Carter, Ashley Douthitt, Robin Osterhout, Aneta Gandjeva, Debbie Slee, Luisa Salter-Cid, Rubin M. Tuder, Lawrence S. Zisman

Selected data previously presented at AHA 2019: Galkin A, Clemons B, Garcia E, Brooks J, Slee D, Salter-Cid L, Zisman L. GB002, A Novel Inhaled PDGFR Kinase Inhibitor, Demonstrates Efficacy in the Su5416 Hypoxia Rat Model of Pulmonary Arterial Hypertension. Circulation 2019;140: A11102; Sitapara R, Slee D, Salter-Cid L, Zisman L. In Vivo Efficacy of a Novel, Inhaled PDGFRα/β Inhibitor, GB002, in the Rat Monocrotaline and Pneumonectomy Model of Pulmonary Arterial Hypertension. Circulation 2019;140: A12947; Galkin A, Sitapara R, Clemons B, Garcia E, Kennedy M, Carter L, Slee D, Salter-Cid L, Zisman L. Pharmacologic Characterization of GB002, a Novel Inhaled PDGFR Kinase Inhibitor in Development for Pulmonary Arterial Hypertension. Eur Resp J 2020; 56:3550.

Take-home message:

Seralutinib is a unique, inhaled, small-molecule kinase inhibitor that targets PDGFRα/β, CSF1R, and c-KIT, and upregulates BMPR2 protein expression; these pathways play important roles in PAH. Efficacy of seralutinib is demonstrated in two animal models of PAH.

Abstract (250 words)

Background: Signaling through platelet-derived growth factor receptor (PDGFR), colony stimulating factor 1 receptor (CSF1R), and c-KIT plays a critical role in pulmonary arterial hypertension (PAH). We examined the preclinical efficacy of inhaled seralutinib, a unique small molecule PDGFR/CSF1R/c-KIT kinase inhibitor in clinical development for PAH, in comparison to a proof-of-concept kinase inhibitor, imatinib.

Methods: Seralutinib and imatinib potency and selectivity were compared. Inhaled seralutinib pharmacokinetics/pharmacodynamics were studied in healthy rats. Efficacy was evaluated in two rat models of PAH: SU5416/Hypoxia (SU5416/H) and monocrotaline pneumonectomy (MCTPN). Effects on inflammatory/cytokine signaling were examined. PDGFR, CSF1R, and c-KIT immunohistochemistry (IHC) in rat and human PAH lung samples and miRNA analysis in the SU5416/H model were performed.

Results: Seralutinib potently inhibited PDGFRα/β, c-KIT and CSF1R. Inhaled seralutinib demonstrated dose-dependent inhibition of lung PDGFR and c-KIT signaling, and increased bone morphogenetic protein receptor type 2 (BMPR2). Seralutinib improved cardiopulmonary hemodynamics and reduced small pulmonary artery muscularization and right ventricle hypertrophy in both models. In the SU5416/H model, seralutinib improved cardiopulmonary hemodynamics, restored lung BMPR2 protein levels, and decreased n-terminal prohormone of brain natriuretic peptide (NT-proBNP) more than imatinib. Quantitative IHC in human lung PAH samples demonstrated increased PDGFR, CSF1R, and c-KIT. miRNA analysis revealed candidates that could mediate seralutinib effects on BMPR2.

Conclusions: Inhaled seralutinib was an effective treatment of severe PAH in two animal models, with improved cardiopulmonary hemodynamics, reduction in NT-proBNP, reverse remodeling of pulmonary vascular pathology, and improvement in inflammatory biomarkers. Seralutinib showed greater efficacy compared to imatinib in a preclinical study.

Introduction

Pulmonary arterial hypertension (PAH) is characterized by perivascular inflammation, proliferation of pulmonary artery smooth muscle cells (PASMCs), myofibroblasts, and endothelial cells (ECs) resulting in pulmonary arterial blood flow obstruction.[1-6] The emergence of apoptosis-resistant cells within pulmonary vascular lesions led to the cancer paradigm hypothesis to explain the abnormal cell proliferation observed in PAH lesions.[1, 4, 5, 7, 8]

Within the context of this cancer-like paradigm, evidence from human PAH lung explants, cell-based assays, and preclinical models points to a pivotal role of platelet-derived growth factor (PDGF) signaling in PAH pathogenesis.[9-14] Expression of PDGF ligands and receptors (PDGFRα/β) was increased in small pulmonary arteries of patients with idiopathic PAH (iPAH) versus controls and PDGFB gene expression was increased in a single-cell RNA sequencing study in iPAH.[11, 15] Genetic knockout studies suggest that PDGFRα and PDGFRβ mediate overlapping and distinct effects across PAH-associated pathways: both receptors regulate cell proliferation, migration, and inflammation, whereas PDGFRβ may uniquely affect angiogenesis.[16] Crosstalk between PDGFR and other signaling cascades implicated in PAH, such as transforming growth factor-beta (TGF-β), has been reported.[17, 18] Furthermore, PDGF signaling decreased BMPR2 expression in PASMCs via miRNA-376b-mediated degradation.[9] These findings highlight the therapeutic potential of PDGFR kinase inhibitors for iPAH.[19]

Imatinib (a potent PDGFR/ABL/c-KIT kinase inhibitor) reversed pulmonary hypertension in the rat monocrotaline model, demonstrating histological and functional improvements.[12] In clinical trials, imatinib improved pulmonary vascular resistance (PVR) and exercise capacity in patients with advanced PAH, however serious adverse events and discontinuations were common, limiting its development as a PAH treatment.[20, 21]

Given the robust evidence implicating PDGFR signaling in PAH pathogenesis and limitations associated with systemic administration of PDGFR inhibitors,[21] seralutinib (N-[3-[(1S)-1-[[6-(3,4-dimethoxyphenyl)pyrazin-2-yl]amino]ethyl]phenyl]-5-methylpyridine-3-carboxamide, formerly PK10571, GB002) was designed and formulated as a dry powder for inhalation drug delivery. In addition to its potent inhibition of PDGFRα and PDGFRβ, seralutinib inhibits PDGFR-related kinases, c-KIT and CSF1R, implicated in PAH pathogenesis and progression.[22-26] c-KIT is expressed on endothelial progenitor cells and mast cells, potentially contributing to perivascular inflammation and vascular remodeling.[8, 23, 27] Increased infiltration of c-KIT-positive cells was observed in pulmonary arterial plexiform lesions in PAH patient lungs.[23] CSF1R is expressed on monocytes and macrophages.[22] Macrophages secrete PDGF ligands and pro-inflammatory cytokines contributing to pathological remodeling in PAH.[24, 25, 28] Thus, a compelling rationale exists to target PDGFR, CSF1R, and c-KIT as a treatment for PAH. Seralutinib targets these pathways and is the first tyrosine kinase inhibitor in clinical development specifically designed as an inhalation therapy for PAH. Given the limitations of imatinib, seralutinib was intentionally developed with low oral bioavailability and rapid clearance characteristics to minimize systemic exposure and associated adverse events. The objectives of the preclinical studies reported here were to investigate the *in vitro* potency and selectivity of seralutinib and characterize its efficacy as compared to imatinib in relevant animal models of PAH.

Methods

The potency and selectivity of seralutinib and imatinib were determined *in vitro*. Pharmacokinetic (PK)/pharmacodynamic (PD) effects of inhaled seralutinib were studied in healthy rats. Efficacy was evaluated in the rat SU5416/H (Study 1 and 3) and MCTPN (Study 2) models. In SU5416/H Study 1, treatment was initiated one day after a three-week hypoxia exposure; in the MCTPN model Study 2, treatment was started on day 25 after pneumonectomy (day 15 after MCT administration). In Study 3, seralutinib or imatinib was started two weeks after return to normoxia, subsequent to the three-week hypoxia period. Treatment effects on echocardiographic parameters, cardiopulmonary hemodynamics, NT-proBNP, BMPR2, and inflammatory markers were examined. PDGFR, CSF1R and c-KIT IHC was performed with rat and human lung PAH and control samples. miRNA analysis of SU5416/H lungs (Study 3) was performed. Detailed methods are in the Online Supplement.

Results

In Vitro **Activity of Seralutinib**

Seralutinib inhibited proliferation of H1703 (PDGFRα-driven cell line), human PASMCs (express similar levels of PDGFRα and PDGFRβ) and human lung fibroblasts (HLF, PDGFRβ>>PDGFRα) with IC50s of 32nM, 33nM, and 29nM, respectively (**Figure 1; Table S1**). Although imatinib inhibited H1703 proliferation with an IC50 of 62nM, its potency was 13–20-fold weaker than seralutinib in human PASMC and HLF proliferation assays. Both compounds potently inhibited PDGF-BB-induced extracellular signal-regulated kinase (ERK) phosphorylation in H1703 cells, however only seralutinib inhibited ERK phosphorylation in HLFs (**Figure 1; Table S1**). Furthermore, seralutinib was more potent than imatinib against c-KIT and CSF1R kinases. Seralutinib inhibited stem-cell factor (SCF)-induced c-KIT autophosphorylation in HPAECs with an IC50 of 7.8 nM and displayed an IC50 of 14.4 nM in M-CSF-induced phosphorylation of CSF1R in human primary differentiated macrophages (34x more potent than imatinib) (**Table S1**, **Figure 1**).

Pharmacokinetic (PK) and Pharmacodynamic Studies

Seralutinib lung concentration peaked immediately after a 2-hour passive inhalation and steadily declined over time in rats. Substantially lower plasma exposures were observed relative to lung exposures. (**Figure 2A**). Four independent rat PK studies demonstrated an average seralutinib lung-to-plasma ratio of 30 (range, 16 to 80) over a 24-hour period. Seralutinib inhalation significantly inhibited PDGF-BB-induced PDGFRα/β autophosphorylation in the lung across all three dose levels tested (**Figure 2B and 2C**). In a separate experiment, with co-administered intratracheal PDGF and SCF, seralutinib inhibited c-KIT Y719 phosphorylation by 43% (**Figure 2D**). Seralutinib inhibition of PDGFRβ phosphorylation in this experiment was similar to that

observed when PDGF-BB was given alone. Furthermore, seralutinib demonstrated a 2-to-2.5-fold dose-dependent increase in lung BMPR2 protein expression over time (**Figure 2E**).

Seralutinib Efficacy in Preclinical Models of PAH

SU5416/H Model (Study 1)

Two cohorts, with and without telemetry monitoring, received seralutinib 2.5 mg/kg and 4.6 mg/kg twice daily (BID), respectively, for two weeks (**Figure 3A**). Prior to initiating treatment, elevated pulmonary artery systolic pressure (PASP) was confirmed in vehicle (100.8±5 mmHg) and seralutinib (99.1±8 mmHg) groups by telemetry. Seralutinib 2.5 mg/kg BID reduced PASP by 43% (P<0.0001) relative to vehicle at the end of treatment. (**Figure 3B**). End-of-study right ventricular systolic pressure (RVSP) measurements revealed dose-dependent reduction with seralutinib (2.5 mg/kg: 49.6 ± 3.1 mmHg, P<0.05; 4.6 mg/kg: 34.7 ± 2.2 mmHg, P<0.001) compared to vehicle (64.4 ± 5.4 mmHg) (**Figure 3C**). Reduction in RV hypertrophy was observed in both seralutinib groups compared to vehicle (**Figure 3D**).

Small pulmonary artery occlusion analysis (vessel diameter < 80 microns) was performed in lung tissues from vehicle and seralutinib 4.6 mg/kg BID groups. A significant decrease was observed in the number of Grade 2 lesions in the seralutinib-treated group compared to vehicle (**Figure 3 E, F**) (P<0.05). Small pulmonary artery lumen-to-media area was increased in the seralutinib-treated group compared to vehicle (P<0.05; **Figure 3G**). IHC of lungs for phospho-PDGFRβ revealed reduced intensity in the seralutinib-treated group compared to vehicle (**Figure 3H**).

MCTPN Model (Study 2)

In this model, seralutinib 2.5 mg/kg BID was initiated after PAH development and continued for 11 days (**Figure 4A**). PASP remained stable in the seralutinib group but continued to increase in

the vehicle group (**Figure 4B**). On days 9, 10, and 11, PASP was 34%, 37%, and 41% lower, respectively, in the seralutinib group compared to vehicle ($P<0.05$). A 50% reduction in RVSP was observed in the seralutinib group compared to vehicle ($P<0.001$) (**Figure 4C**). RV hypertrophy was reduced by 49% in the seralutinib group compared to vehicle ($P<0.0001$) (**Figure 4D**). Lumen-to-media area was increased in the seralutinib-treated group compared to controls, which indicated favorable reverse remodeling ($P<0.001$) (**Figure 4E, F**), with fewer Grade 1 and 2 lesions (**Figure 4 E, GG**). A qualitative decrease in perivascular fibrosis was observed in seralutinib-treated lungs compared to vehicle (**Figure S1**).

Seralutinib significantly improved tidal volume ($P<0.005$) and decreased respiratory rate ($P<0.001$) as compared to vehicle (**Figure S2A, B**). Minute ventilation and airway resistance were similar between seralutinib- and vehicle-treated animals (**Figure S2C, D**).

SU5416/H Model (Study 3): Comparison to Imatinib

Seralutinib (12.8 mg/kg BID) or imatinib (15.0 mg/kg) was administered for two weeks following disease induction and a two-week period of normoxia (**Figure 5A**). The imatinib dose selected for the *in vivo* study displayed potent inhibition of PDGFR phosphorylation in healthy rats (**Figure S3**).

At treatment initiation, disease severity was evaluated by echocardiography. Stroke volume index (SVI) and cardiac index (CI) were decreased in diseased animals compared to healthy controls (**Figure 5B**). Vehicle-treated PAH rats had an elevated mean pulmonary artery pressure (mPAP) (50.9 ± 5.0 mmHg) and RVSP (85.2 ± 11.0 mmHg) compared to healthy controls (mPAP 12.6 ± 0.6 mmHg; RVSP 19.5 ± 1.0 mmHg, (**Figure 5B, C**). Seralutinib improved echocardiographic and hemodynamic parameters, with reductions of 37% and 45% in mPAP

(31.9±2.6 mmHg) and RVSP (46.7±3.9 mmHg), respectively, compared to vehicle (*P*<0.001, **Figure 5B, C**). The decrease in mPAP and improvement in CI resulted in a 60% improvement in PVR index (PVRI) in the seralutinib group (*P*<0.0001, **Figure 5C**). Imatinib reduced mPAP by 27% (37.4±3.9 mmHg) and RVSP by 28% (61.1±7.4 mmHg) (*P*<0.05 vs. vehicle, **Figure 5B, C**). Compared to imatinib, seralutinib effected a significantly greater effect on SVI and CI (**Figure 5B**). The reduction in PVRI from imatinib treatment was approximately 37%. Disease induction increased NT-proBNP by 9-fold. Seralutinib decreased NT-proBNP by 55% (*P*<0.05), while no significant effect was observed with imatinib (**Figure 5C**). Although the effects of seralutinib on these parameters were statistically greater than the effects of imatinib compared to vehicle, there was no statistically significant difference between seralutinib and imatinib with regard to mPAP, RVSP, PVRI or NT-proBNP.

Hemodynamic improvements were accompanied by a decrease in small pulmonary vessel muscularization (**Figure 5D, E**). Analysis of H&E-stained lung sections, and α-smooth muscle actin (SMA)-stained sections demonstrated a decrease in small pulmonary artery muscularization in the seralutinib group compared to both the vehicle and imatinib-treated groups (**Figure 5D, E, and Figure S4**). Seralutinib significantly increased BMPR2, whereas no significant effect on BMPR2 was observed with imatinib (**Figure 5E**). An increase in SMAD1/5 phosphorylation in seralutinib-treated animals was observed, suggesting activation of signaling through BMPR2 (**Figure S5**).

Effects on biomarkers of inflammation

Seralutinib decreased circulating levels of plasma tumor necrosis factor alpha (TNFα) (*P*<0.001) and increased interleukin (IL)-10 compared to vehicle (*P*<0.05, **Figure 6A, B**). Imatinib did not

significantly alter IL-10 or TNFα levels. A trend towards decreased PDGF-BB was observed in the seralutinib-treated group (**Figure 6C**). Seralutinib also decreased lung mRNA and protein levels of MCP-1 (a pro-inflammatory cytokine that regulates macrophage recruitment and contributes to MCT-induced pulmonary hypertension[29]) (SU5416/H model: P<0.05 compared to vehicle) (**Figure S6B-C**). Imatinib did not modulate MCP1. Seralutinib reduced MCP-1 secretion in a dose-dependent manner in CSF1R+ human macrophages. (**Figure S6A**).

Effect of seralutinib on microRNAs in the lung

Six miRNAs predicted to repress both human and rat BMPR2 were differentially expressed in seralutinib-treated SU5416/H rat lungs relative to vehicle (**Table S2**). Two of the six miRNAs decreased following treatment with seralutinib (miR135-5p, p=0.01 and miR146a-5p, p=0.02), consistent with the observed increase of BMPR2 protein (**Figure 5E).** Four miRNAs were increased by seralutinib including miR381-3p, which exhibited the largest expression shift and was significantly higher in seralutinib and imatinib groups relative to vehicle.

Immunohistochemistry in IPAH vs. Control Lungs

We evaluated expression of PDGFRα/β, c-KIT and CSF1R across human lung tissue samples to demonstrate relevance of seralutinib targets in iPAH (**Figure 7**). Increased PDGFRα, PDGFRβ, c-KIT and CSF1R in PAH lung sections was observed compared to controls. IHC in rat lungs from the MCTPN and SU5416/H models showed patterns of PDGFRα/β and CSF1R similar to that seen in human PAH samples (**Figures S7 and S8**). In both animal models, treatment with seralutinib was associated with decreased signal for PDGFRα/β and CSF1R.

Discussion

PDGFR, CSF1R, and c-KIT signaling play crucial roles in the pathology and progression of PAH. [9-15, 21-26, 30, 31] Targeting these pathways therefore holds promise as a therapeutic strategy in PAH. Seralutinib is a highly potent PDGFR, CSF1R, and c-KIT kinase inhibitor, and is the first and only tyrosine kinase inhibitor intentionally designed as a treatment for PAH. Seralutinib's unique physical properties make it suitable for the inhaled route of administration, potentially optimizing therapeutic efficacy whilst limiting systemic exposure and associated side effects.

Clinical trials of imatinib in PAH provided proof of concept that targeting PDGFR signaling can impact PAH disease progression.[21] However, further development of imatinib was limited due to side effects attributable to relatively high systemic exposure. The clinical experience with imatinib provided impetus and rationale to develop a tyrosine kinase inhibitor targeting pathways relevant to PAH and optimized for delivery directly to the diseased lung by inhalation.

In addition to its optimization for inhaled delivery, seralutinib displays several other unique features compared to imatinib. For example, only seralutinib inhibited ERK phosphorylation in HLFs. This difference could be important because constitutive activation of ERK1/2 has been shown to be a driver of proliferation in BMPR2-silenced PAH-derived cells.[32] Seralutinib showed a 13- to 20-fold greater potency at inhibiting proliferation in human PASMCs and HLFs compared to imatinib. Furthermore, seralutinib was more potent than imatinib against c-KIT and CSF1R kinases. A limitation of the current data is the absence of compound profiling in patient-derived cells. PAH-derived PASMCs and HLFs display altered metabolism and functional signaling compared to healthy cells.[33] [34] Future studies using PAH patient cells could provide additional insights into the effects of these compounds.

Two animal models of PAH were used to examine the efficacy of inhaled seralutinib: the SU5416/H model and the MCTPN model. The SU5416/H model reproduces significant features of human PAH, including angio-obliterative lesions and vascular remodeling.[35] The MCTPN model is associated with increased inflammation, fibrosis, increased PAP, and obstructive neointimal lesions (a feature not observed in the MCT-only model).[36, 37] While it is recognized that the results of drug studies performed in animal models of PAH do not necessarily translate to human disease, the models we studied replicate key features and different aspects of human PAH. Furthermore, the experiments were designed to demonstrate a therapeutic effect after pulmonary hypertension was established rather than a preventive strategy.

Seralutinib prevented PAH progression in the MCTPN model and reversed pulmonary hypertension in the SU5416/H model in a dose-responsive manner. Hemodynamic improvements were accompanied by reverse pulmonary vascular remodeling, a reduction in NT-proBNP, an increase in pulmonary BMPR2, and an improvement in inflammatory biomarkers. The pathways targeted directly or indirectly by seralutinib stand out as key regulatory nodes in the pathological remodeling associated with PAH (**Figure 8**). In our head-to-head preclinical study, both seralutinib and imatinib decreased mPAP, RVSP, PVRI and NT-proBNP compared to vehicle; however, the effects of seralutinib were more statistically robust. In addition, seralutinib had a greater effect in restoring small pulmonary artery muscularization towards normal compared to imatinib. Interestingly, BMPR2 was restored to normal levels in the seralutinib-treated group, but not in the imatinib-treated group. Furthermore, while seralutinib decreased MCP-1 (CCL2), imatinib did not. Differences in compound potency, kinase selectivity, and downstream signaling profiles as well as target coverage *in vivo* could be contributing to the observed differences between seralutinib and imatinib.

Seralutinib is a more potent PDGFRβ inhibitor than imatinib. Because signaling through PDGFRα and PDGFRβ may mediate different effects important in pathological pulmonary vascular remodeling, potent inhibition of both kinases may lead to improved efficacy *in vivo*. Seralutinib is also a strikingly more potent inhibitor of CSF1R than imatinib, potentially contributing to reduced inflammation and reverse remodeling. In seralutinib-treated animals in the MCTPN study, inhibition of both PDGFR and CSF1R signaling pathways may be contributing to the observed reduction in peri-vascular fibrosis. Although we cannot rule out that down-modulation of inflammatory markers observed in the current study may be an indirect outcome of seralutinib's reverse remodeling effects, MCP1 modulation has been directly linked to CSF1R signal transduction in human macrophages,[38, 39] and would therefore be indicative of seralutinib target engagement. Future studies to evaluate the potential anti-inflammatory and anti-fibrotic properties of seralutinib would be of interest.

Loss of BMPR2 plays a pivotal role in the pathogenesis of PAH and crosstalk between PDGFR signaling and BMPR2 expression has been reported.[9] miRNAs can mediate crosstalk between PDGFR signaling and BMPR2, directly by repressing BMPR2 expression or indirectly by repressing other targets which alter BMPR2.[40-42] We identified six miRNA predicted to suppress both rat and human BMPR2 that were differentially expressed in SU5416/H rats treated with seralutinib. MiR135a-5p and miR146a-5p were decreased in seralutinib-treated lungs, consistent with the observed BMPR2 increase. Mir135a has previously been implicated in human pulmonary hypertension [42, 43] and linked to BMPR2-specific expression in animal models.[41, 44] For example, in the mouse OVA/PM model of PAH, treatment with Antago-miR135a restored BMPR2 to levels observed in healthy lungs.[41] A limitation of our study is that mir135a-5p expression was only detected in one out of four animals treated with imatinib, which suggests

this miRNA may not be the sole contributor to the observed changes in BMPR2 in the seralutinib group (since BMPR2 in the imatinib group was unchanged). Mir146a-5p expression, decreased with seralutinib in our study, was increased in serum from PAH patients relative to healthy controls, and has been shown to promote proliferation in HPAECs.[45] Although miR-376b was reported to be regulated by PDGF-BB, we did not find a significant regulation of this miRNA in our model.[9] Several additional predicted BMPR2-regulating miRNAs were elevated following treatment with seralutinib, (i.e., predicted to reduce BMPR2 protein expression). For example, miR-381-3p, was strongly upregulated in the seralutinib and imatinib groups compared to vehicle. miR-381-3p is predicted to weakly repress BMPR2 but also functions as a tumor suppressor, blocking proliferation in cancer cell lines.[46] Furthermore, increased miR-381-3p has been shown to repress TGFβ and inhibits proliferation of human bronchial smooth muscle cells.[47] The net effect on BMPR2 expression of these miRNAs as an ensemble has not been characterized and is difficult to predict. Future studies could shed light on the contribution of each miRNA to seralutinib's mechanism of action. Regardless of mechanism, the increase in BMPR2 following seralutinib treatment could lead to synergistic effects in combination with therapeutic approaches specifically targeting the activin/TGFβ pathway.

Seralutinib is also a potent c-KIT inhibitor and decreased SCF-induced autophosphorylation of KIT in HPAECs. Hypoxia was shown to increase c-KIT expression on pulmonary ECs, enhancing the angiogenic response to SCF and contributing to pulmonary vascular pathology in the SU5416/H rat model.[26] Infiltration of c-KIT positive cells (endothelial progenitor cells and mast cells) was also reported in pulmonary arterial plexiform lesions in PAH lungs.[8, 23, 27, 48] Lung-targeted delivery of seralutinib may mitigate risks associated with systemic c-KIT inhibition by limiting inhibition to the disease site.

Quantitative IHC demonstrated increased integrated intensity of PDGFRα, PDGFRβ, c-KIT, and CSF1R in human PAH lungs compared to controls. Our findings are consistent with previous reports of increased expression of PDGFRα, PDGFRβ, and c-KIT in human PAH lungs.[11, 23] To our knowledge this is the first report of increased CSF1R expression in human PAH. These findings support the relevance of targeting CSF1R in addition to PDGFRs, and c-KIT in PAH. IHC of PDGFRα/β and CSF1R in both the rat MCTPN and SU5416/H models showed patterns similar to that seen in human PAH.

In conclusion, seralutinib delivered as an inhaled dry powder was shown to be effective in two preclinical models of PAH. As these animal models of PAH replicate different features of the human disease, the fact that seralutinib demonstrated robust efficacy in both models increases the likelihood of seralutinib's efficacy as a treatment in human PAH. The improvement in BMPR2 levels observed with seralutinib is consistent with the reverse remodeling of small pulmonary arteries in PAH. Current standard of care treatments in PAH function primarily as vasodilators, with limited effects on neointimal proliferation and pulmonary vascular remodeling. Our studies indicate that seralutinib has a direct ameliorative impact on pulmonary vascular remodeling that results in improved cardiopulmonary hemodynamics. The design of these studies ensured that seralutinib was initiated under fully established disease conditions, thus demonstrating the potential for efficacy in a therapeutic setting. Observed reverse remodeling of the small pulmonary arteries and restoration of lung BMPR2 expression in the rat PAH models suggest that seralutinib may impact underlying causes of PAH. Seralutinib is currently in clinical development for patients with PAH (NCT04456998).

Acknowledgments

References

1. Cool CD, Kuebler WM, Bogaard HJ, et al. The hallmarks of severe pulmonary arterial hypertension: the cancer hypothesis-ten years later. *Am J Physiol Lung Cell Mol Physiol* 2020; 318: L1115-L1130. 2020/02/06. DOI: 10.1152/ajplung.00476.2019.

2. El Chami H and Hassoun PM. Inflammatory mechanisms in the pathogenesis of pulmonary arterial hypertension. *Compr Physiol* 2011; 1: 1929-1941. 2011/10/01. DOI: 10.1002/cphy.c100028.

3. Humbert M and Hoeper MM. Severe pulmonary arterial hypertension: a forme fruste of cancer? *Am J Respir Crit Care Med* 2008; 178: 551-552. 2008/08/30. DOI: 10.1164/rccm.200806-867ED.

4. Pullamsetti SS, Savai R, Seeger W, et al. Translational Advances in the Field of Pulmonary Hypertension. From Cancer Biology to New Pulmonary Arterial Hypertension Therapeutics. Targeting Cell Growth and Proliferation Signaling Hubs. *Am J Respir Crit Care Med* 2017; 195: 425-437. 2016/09/15. DOI: 10.1164/rccm.201606-1226PP.

5. Rai PR, Cool CD, King JA, et al. The cancer paradigm of severe pulmonary arterial hypertension. *Am J Respir Crit Care Med* 2008; 178: 558-564. 2008/06/17. DOI: 10.1164/rccm.200709-1369PP.

6. Stacher E, Graham BB, Hunt JM, et al. Modern age pathology of pulmonary arterial hypertension. *Am J Respir Crit Care Med* 2012; 186: 261-272. 2012/06/09. DOI: 10.1164/rccm.201201-0164OC.

7. Boucherat O, Vitry G, Trinh I, et al. The cancer theory of pulmonary arterial hypertension. *Pulm Circ* 2017; 7: 285-299. 2017/06/10. DOI: 10.1177/2045893217701438.

8.   Jonigk D, Golpon H, Bockmeyer CL, et al. Plexiform lesions in pulmonary arterial hypertension composition, architecture, and microenvironment. *Am J Pathol* 2011; 179: 167-179. 2011/06/28. DOI: 10.1016/j.ajpath.2011.03.040.

9.   Chen J, Cui X, Qian Z, et al. Multi-omics analysis reveals regulators of the response to PDGF-BB treatment in pulmonary artery smooth muscle cells. *BMC Genomics* 2016; 17: 781. 2016/10/08. DOI: 10.1186/s12864-016-3122-3.

10.   Grimminger F and Schermuly RT. PDGF receptor and its antagonists: role in treatment of PAH. *Adv Exp Med Biol* 2010; 661: 435-446. 2010/03/06. DOI: 10.1007/978-1-60761-500-2_28.

11.   Perros F, Montani D, Dorfmuller P, et al. Platelet-derived growth factor expression and function in idiopathic pulmonary arterial hypertension. *Am J Respir Crit Care Med* 2008; 178: 81-88. 2008/04/19. DOI: 10.1164/rccm.200707-1037OC.

12.   Schermuly RT, Dony E, Ghofrani HA, et al. Reversal of experimental pulmonary hypertension by PDGF inhibition. *J Clin Invest* 2005; 115: 2811-2821. 2005/10/04. DOI: 10.1172/JCI24838.

13.   Stavri GT, Hong Y, Zachary IC, et al. Hypoxia and platelet-derived growth factor-BB synergistically upregulate the expression of vascular endothelial growth factor in vascular smooth muscle cells. *FEBS Lett* 1995; 358: 311-315. 1995/01/30. DOI: 10.1016/0014-5793(94)01458-d.

14.   Ten Freyhaus H, Berghausen EM, Janssen W, et al. Genetic Ablation of PDGF-Dependent Signaling Pathways Abolishes Vascular Remodeling and Experimental Pulmonary Hypertension. *Arterioscler Thromb Vasc Biol* 2015; 35: 1236-1245. 2015/03/07. DOI: 10.1161/ATVBAHA.114.304864.

15.   Saygin D, Tabib T, Bittar HET, et al. Transcriptional profiling of lung cell populations in idiopathic pulmonary arterial hypertension. *Pulm Circ* 2020; 10 2020/03/14. DOI: 10.1177/2045894020908782.

16.   Wu E, Palmer N, Tian Z, et al. Comprehensive dissection of PDGF-PDGFR signaling pathways in PDGFR genetically defined cells. *PLoS One* 2008; 3: e3794. 2008/11/26. DOI: 10.1371/journal.pone.0003794.

17.   Kudryashova TV, Shen Y, Pena A, et al. Inhibitory Antibodies against Activin A and TGF-beta Reduce Self-Supported, but Not Soluble Factors-Induced Growth of Human Pulmonary Arterial Vascular Smooth Muscle Cells in Pulmonary Arterial Hypertension. *Int J Mol Sci* 2018; 19 2018/10/03. DOI: 10.3390/ijms19102957.

18.   Porsch H, Mehic M, Olofsson B, et al. Platelet-derived growth factor beta-receptor, transforming growth factor beta type I receptor, and CD44 protein modulate each other's signaling and stability. *J Biol Chem* 2014; 289: 19747-19757. 2014/05/27. DOI: 10.1074/jbc.M114.547273.

19.   Atkinson C, Stewart S, Upton PD, et al. Primary pulmonary hypertension is associated with reduced pulmonary vascular expression of type II bone morphogenetic protein receptor. *Circulation* 2002; 105: 1672-1678. 2002/04/10. DOI: 10.1161/01.cir.0000012754.72951.3d.

20.   Ghofrani HA, Morrell NW, Hoeper MM, et al. Imatinib in pulmonary arterial hypertension patients with inadequate response to established therapy. *Am J Respir Crit Care Med* 2010; 182: 1171-1177. 2010/06/29. DOI: 10.1164/rccm.201001-0123OC.

21.   Hoeper MM, Barst RJ, Bourge RC, et al. Imatinib mesylate as add-on therapy for pulmonary arterial hypertension: results of the randomized IMPRES study. *Circulation* 2013; 127: 1128-1138. 2013/02/14. DOI: 10.1161/CIRCULATIONAHA.112.000765.

22. Stanley ER and Chitu V. CSF-1 receptor signaling in myeloid cells. *Cold Spring Harb Perspect Biol* 2014; 6 2014/06/04. DOI: 10.1101/cshperspect.a021857.

23. Montani D, Perros F, Gambaryan N, et al. C-kit-positive cells accumulate in remodeled vessels of idiopathic pulmonary arterial hypertension. *Am J Respir Crit Care Med* 2011; 184: 116-123. 2011/04/08. DOI: 10.1164/rccm.201006-0905OC.

24. Abid S, Marcos E, Parpaleix A, et al. CCR2/CCR5-mediated macrophage-smooth muscle cell crosstalk in pulmonary hypertension. *Eur Respir J* 2019; 54 2019/07/20. DOI: 10.1183/13993003.02308-2018.

25. Sheikh AQ, Saddouk FZ, Ntokou A, et al. Cell Autonomous and Non-cell Autonomous Regulation of SMC Progenitors in Pulmonary Hypertension. *Cell Rep* 2018; 23: 1152-1165. 2018/04/26. DOI: 10.1016/j.celrep.2018.03.043.

26. Farkas D, Kraskauskas D, Drake JI, et al. CXCR4 inhibition ameliorates severe obliterative pulmonary hypertension and accumulation of C-kit(+) cells in rats. *PLoS One* 2014; 9: e89810. 2014/03/04. DOI: 10.1371/journal.pone.0089810.

27. Toshner M, Voswinckel R, Southwood M, et al. Evidence of dysfunction of endothelial progenitors in pulmonary arterial hypertension. *Am J Respir Crit Care Med* 2009; 180: 780-787. 2009/07/25. DOI: 10.1164/rccm.200810-1662OC.

28. Joshi N, Watanabe S, Verma R, et al. A spatially restricted fibrotic niche in pulmonary fibrosis is sustained by M-CSF/M-CSFR signalling in monocyte-derived alveolar macrophages. *Eur Respir J* 2020; 55 2019/10/12. DOI: 10.1183/13993003.00646-2019.

29. Ikeda Y, Yonemitsu Y, Kataoka C, et al. Anti-monocyte chemoattractant protein-1 gene therapy attenuates pulmonary hypertension in rats. *Am J Physiol Heart Circ Physiol* 2002; 283: H2021-2028. 2002/10/18. DOI: 10.1152/ajpheart.00919.2001.

30.   Savai R, Pullamsetti SS, Kolbe J, et al. Immune and inflammatory cell involvement in the pathology of idiopathic pulmonary arterial hypertension. *Am J Respir Crit Care Med* 2012; 186: 897-908. 2012/09/08. DOI: 10.1164/rccm.201202-0335OC.

31.   Talati M, West J, Zaynagetdinov R, et al. BMP pathway regulation of and by macrophages. *PLoS One* 2014; 9: e94119. 2014/04/10. DOI: 10.1371/journal.pone.0094119.

32.   Awad KS, Elinoff JM, Wang S, et al. Raf/ERK drives the proliferative and invasive phenotype of BMPR2-silenced pulmonary artery endothelial cells. *Am J Physiol Lung Cell Mol Physiol* 2016; 310: L187-201. 2015/11/22. DOI: 10.1152/ajplung.00303.2015.

33.   Wu K, Tang H, Lin R, et al. Endothelial platelet-derived growth factor-mediated activation of smooth muscle platelet-derived growth factor receptors in pulmonary arterial hypertension. *Pulm Circ* 2020; 10: 2045894020948470. 2020/12/10. DOI: 10.1177/2045894020948470.

34.   Barnes JW, Tian L, Heresi GA, et al. O-linked beta-N-acetylglucosamine transferase directs cell proliferation in idiopathic pulmonary arterial hypertension. *Circulation* 2015; 131: 1260-1268. 2015/02/11. DOI: 10.1161/CIRCULATIONAHA.114.013878.

35.   Taraseviciene-Stewart L, Kasahara Y, Alger L, et al. Inhibition of the VEGF receptor 2 combined with chronic hypoxia causes cell death-dependent pulmonary endothelial cell proliferation and severe pulmonary hypertension. *FASEB J* 2001; 15: 427-438. 2001/02/07. DOI: 10.1096/fj.00-0343com.

36.   Okada K, Tanaka Y, Bernstein M, et al. Pulmonary hemodynamics modify the rat pulmonary artery response to injury. A neointimal model of pulmonary hypertension. *Am J Pathol* 1997; 151: 1019-1025. 1997/11/05.

37.   White RJ, Meoli DF, Swarthout RF, et al. Plexiform-like lesions and increased tissue factor expression in a rat model of severe pulmonary arterial hypertension. *Am J Physiol Lung Cell Mol Physiol* 2007; 293: L583-590. 2007/06/26. DOI: 10.1152/ajplung.00321.2006.

38.   Bellamri N, Morzadec C, Joannes A, et al. Alteration of human macrophage phenotypes by the anti-fibrotic drug nintedanib. *Int Immunopharmacol* 2019; 72: 112-123. 2019/04/12. DOI: 10.1016/j.intimp.2019.03.061.

39.   Wlodarczyk A, Benmamar-Badel A, Cedile O, et al. CSF1R Stimulation Promotes Increased Neuroprotection by CD11c+ Microglia in EAE. *Front Cell Neurosci* 2018; 12: 523. 2019/01/29. DOI: 10.3389/fncel.2018.00523.

40.   Brock M, Trenkmann M, Gay RE, et al. Interleukin-6 modulates the expression of the bone morphogenic protein receptor type II through a novel STAT3-microRNA cluster 17/92 pathway. *Circ Res* 2009; 104: 1184-1191. 2009/04/25. DOI: 10.1161/CIRCRESAHA.109.197491.

41.   Lee HW and Park SH. Elevated microRNA-135a is associated with pulmonary arterial hypertension in experimental mouse model. *Oncotarget* 2017; 8: 35609-35618. 2017/04/19. DOI: 10.18632/oncotarget.16011.

42.   Santos-Ferreira CA, Abreu MT, Marques CI, et al. Micro-RNA Analysis in Pulmonary Arterial Hypertension: Current Knowledge and Challenges. *JACC Basic Transl Sci* 2020; 5: 1149-1162. 2020/12/10. DOI: 10.1016/j.jacbts.2020.07.008.

43.   Parikh VN, Jin RC, Rabello S, et al. MicroRNA-21 integrates pathogenic signaling to control pulmonary hypertension: results of a network bioinformatics approach. *Circulation* 2012; 125: 1520-1532. 2012/03/01. DOI: 10.1161/CIRCULATIONAHA.111.060269.

44.   Liu HM, Jia Y, Zhang YX, et al. Dysregulation of miR-135a-5p promotes the development of rat pulmonary arterial hypertension in vivo and in vitro. *Acta Pharmacol Sin* 2019; 40: 477-485. 2018/07/25. DOI: 10.1038/s41401-018-0076-9.

45.   Zhang W, Qi Y and Wu B. MicroRNA-146-5p Promotes Pulmonary Artery Endothelial Cell Proliferation under Hypoxic Conditions through Regulating USP3. *Dis Markers* 2021; 2021: 3668422. 2021/12/18. DOI: 10.1155/2021/3668422.

46.   Yu YZ, Mu Q, Ren Q, et al. miR-381-3p suppresses breast cancer progression by inhibition of epithelial-mesenchymal transition. *World J Surg Oncol* 2021; 19: 230. 2021/08/08. DOI: 10.1186/s12957-021-02344-w.

47.   Bai SY, Li ML, Ren Y, et al. HDAC8-inhibitor PCI-34051-induced exosomes inhibit human bronchial smooth muscle cell proliferation via miR-381-3p mediated TGFB3. *Pulm Pharmacol Ther* 2021; 71: 102096. 2021/11/07. DOI: 10.1016/j.pupt.2021.102096.

48.   Stearman RS, Bui QM, Speyer G, et al. Systems Analysis of the Human Pulmonary Arterial Hypertension Lung Transcriptome. *Am J Respir Cell Mol Biol* 2019; 60: 637-649. 2018/12/19. DOI: 10.1165/rcmb.2018-0368OC.

Figure legends

H1703
Constitutively active PDGFRα

% Proliferation vs Log Compound (M)

IC$_{50}$
seralutinib 32 nM
imatinib 62 nM

H1703 (PDGFRα)
PDGFB→pERK

% pERK vs Log Compound (M)

IC$_{50}$
seralutinib 74 nM
imatinib 268 nM

HPASMC (PDGFRα=β)
PDGFB→Proliferation

% PDGFB-Induced Proliferation vs Log Compound [M]

IC$_{50}$
seralutinib 33 nM
imatinib 419 nM

D0

HPASMC (PDGFRβ=α)
PDGFB→pERK

% pERK vs Log Compound (M)

IC$_{50}$
seralutinib 49 nM
imatinib 2300 nM

HLF (PDGFRβ>α)
PDGFB→Proliferation

% PDGFB-Induced Proliferation vs Log Compound (M)

IC$_{50}$
seralutinib 29 nM
imatinib 579 nM

HLF (PDGFRβ>α)
PDGFB→pERK

% pERK vs Log Compound (M)

IC$_{50}$
seralutinib 62 nM
imatinib >10 μM

HPAEC (c-KIT)
SCF→pcKIT

% phospho-c-KIT/totalc-KIT vs Log Compound (M)

IC$_{50}$
seralutinib 7.8 nM
imatinib 301 nM

Mφ Human Macrophage (CSF1R)
M-CSF→phospho CSF1R

% pCSF1R/ tCSF1R vs Log Compound (M)

IC$_{50}$
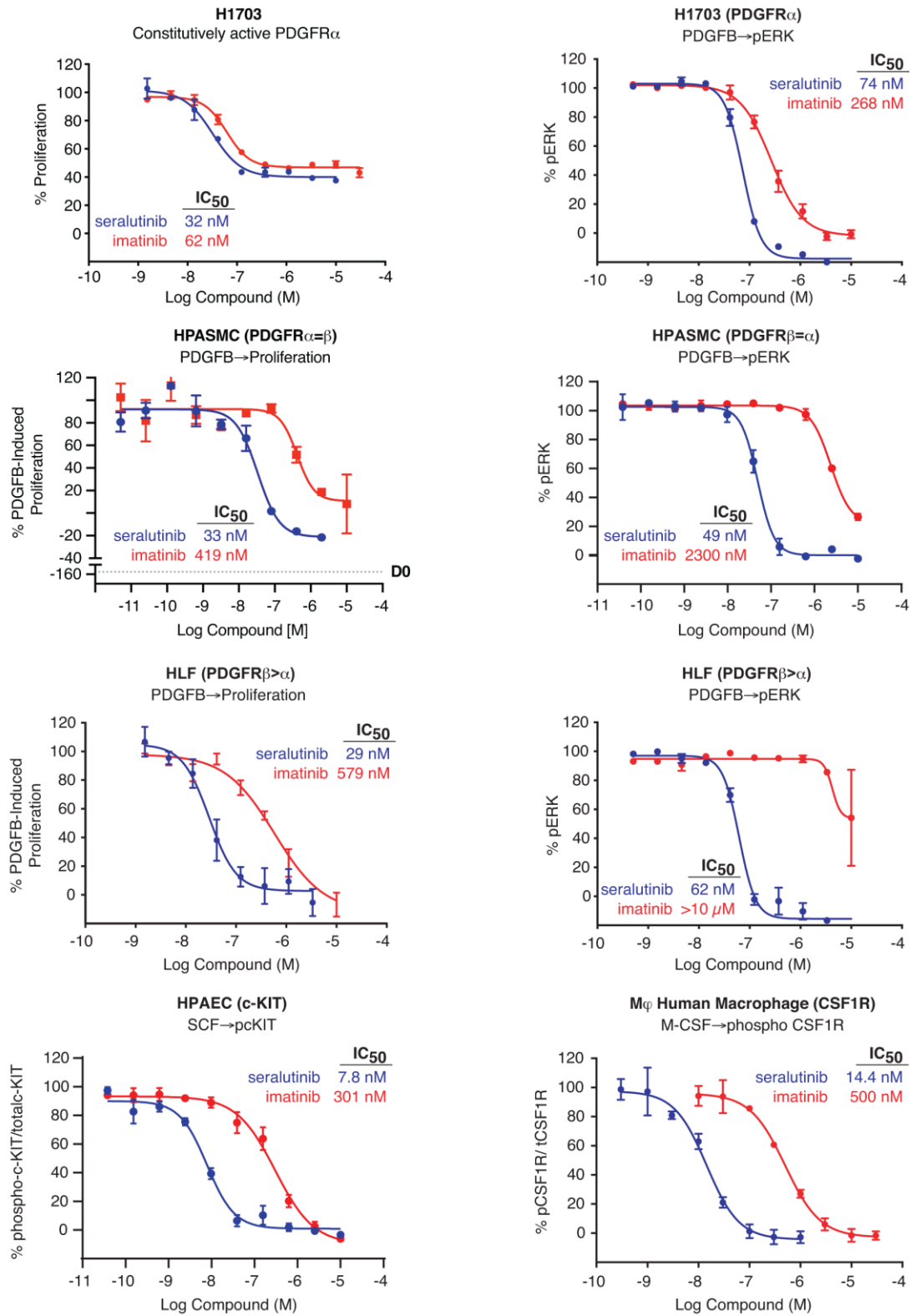seralutinib 14.4 nM
imatinib 500 nM

Figure 1. In vitro cell-based potency of seralutinib versus imatinib. Inhibition of constitutively active PDGFRα-driven proliferation in a human lung epithelial cell line (H1703), or PDGF-BB-induced proliferation in human pulmonary arterial smooth muscle cells (HPASMC) and human lung fibroblast (HLF) cells was measured using CyQuant® or CellTiter-Glo® Assay. The values for each concentration are normalized to 3 days of PDGFB stimulation (considered 100% proliferation) and no stimulation for day 3 (0% proliferation). For the HPASMC proliferation assay D0 represents the basal value at day 0 just prior to PDGFB stimulation. Inhibition of PDGF-BB induced phosphorylation of ERK in H1703 and HLF cells was measured using homogeneous time resolved fluorescence (HTRF) assay. Inhibition of SCF-induced phosphorylation of c-KIT in human pulmonary artery endothelial cells (HPAEC), and M-CSF induced phosphorylation of CSF1R in human primary macrophages was measured using ELISA. Error bars represent the standard deviation of duplicate or triplicate measurements. Data presented as mean nanomolar IC50 values for seralutinib (blue) and imatinib (red). PDGF-B = PDGF-BB.
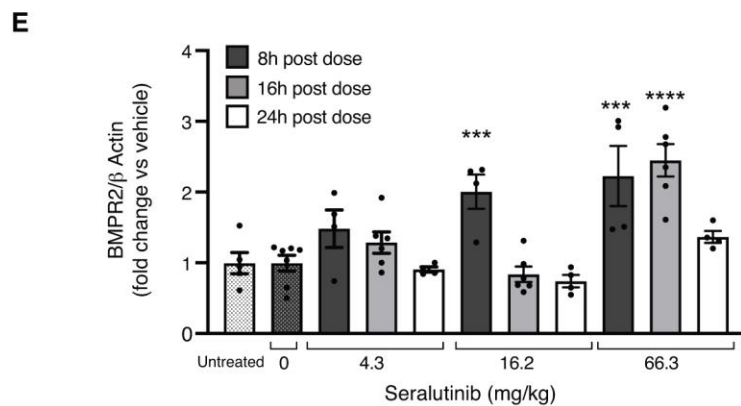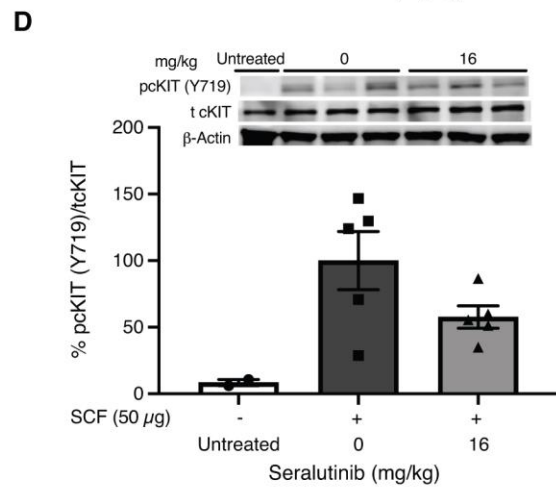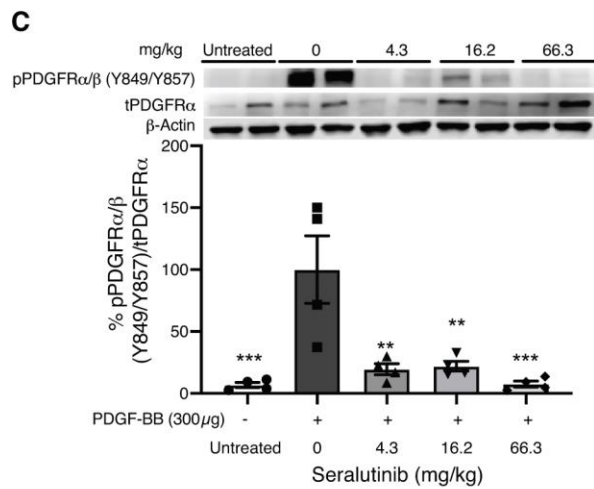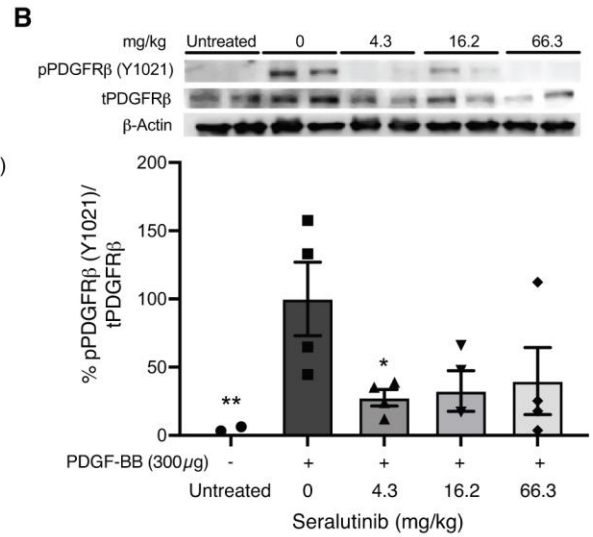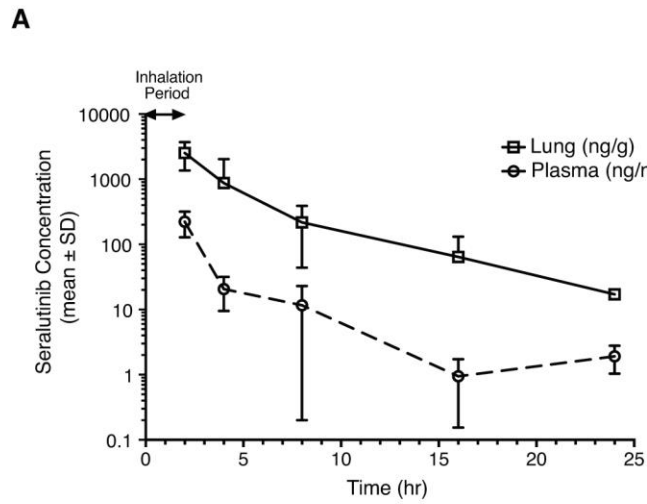
Figure 2. Seralutinib *in vivo* pharmacokinetic (PK)/pharmacodynamic (PD) profile. Male SD rats received vehicle or seralutinib 4.3 mg/kg, 16.2 mg/kg, and 66.3 mg/kg via passive inhalation. (*A*) Seralutinib concentrations in lung (square) and plasma (circle) over 24 hours post 4.3 mg/kg passive inhalation. For PD readout in lungs, rats were administered PDGF-BB and SCF via intratracheal insufflation into the lungs immediately post-dosing. Five minutes post-challenge, lungs were harvested to measure phosphorylation of PDGFR and c-KIT. Data presented as percent change in *(B)* phospho PDGFRβ (Y1021)/ total PDGFRβ, *(C)* phospho PDGFRα/β (Tyr849/Tyr857)/ PDGFRα, and *(D)* phospho c-KIT/total c-KIT in lung homogenates by western blot analysis. *(E)* Mean fold change in lung BMPR2/β-Actin protein expression at 8, 16 and 24 hours post-seralutinib dosing. Data presented as mean ± SEM (n=4 for A-C, n=2 to 5 for D, n=4 to 8 for E). Statistical analysis was performed using one-way analysis of variance with Dunnett's multiple comparisons test. *$P<0.05$, **$P<0.005$ and *** $P<0.001$, seralutinib versus vehicle treatment group.
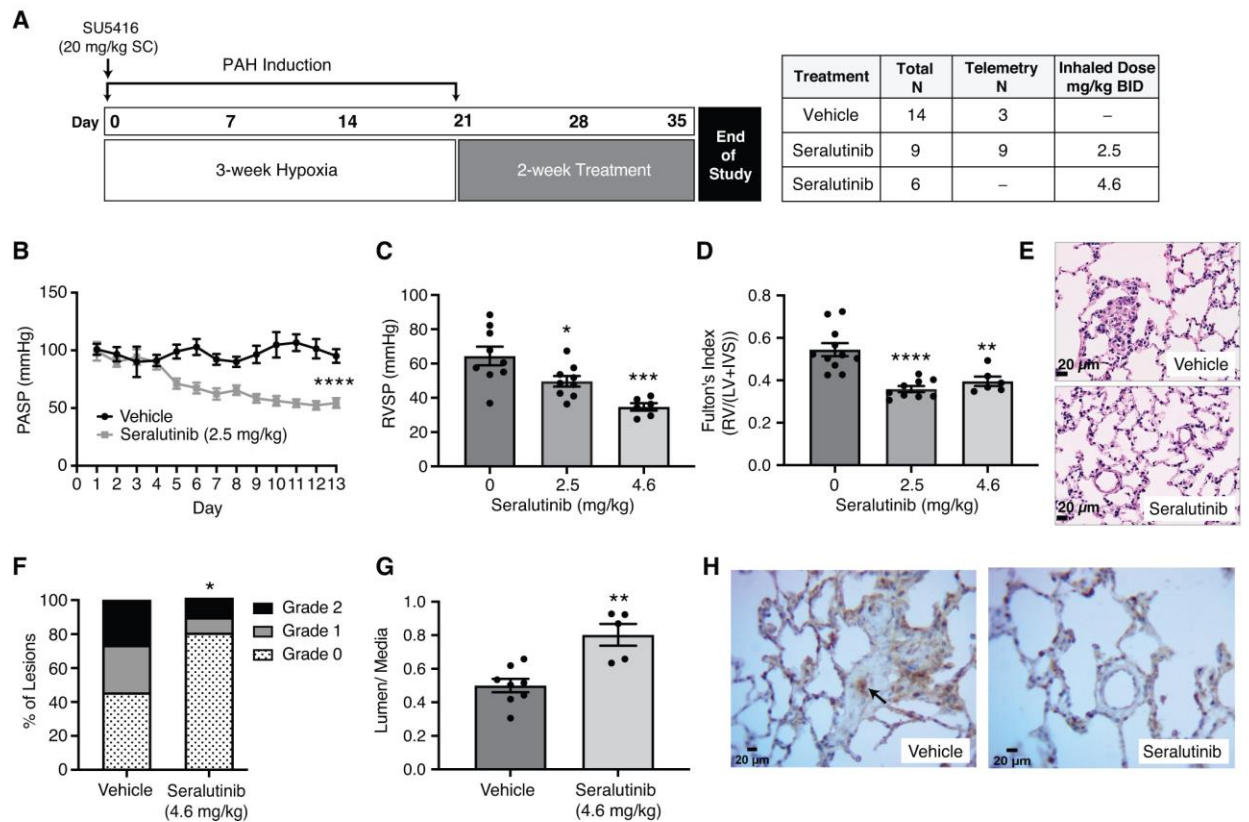
Figure 3. Inhaled seralutinib efficacy in SU5416/H model of pulmonary arterial hypertension.

(*A*) SU5416/H model dose-response and telemetry study schema. (*B*) Pulmonary artery systolic

pressure (PASP) measured by implanted telemetry device following vehicle (black circle) and

seralutinib 2.5 mg/kg (grey square) over the course of treatment. *(C)* Change in right ventricular

systolic pressure (RVSP) and *(D)* right ventricle hypertrophy measured by Fulton's index by

treatment. *(E)* Representative photomicrograph of immunohistological changes in lung by H & E

stain, scale bars, 20μm. *(F)* Occlusive grading analysis of pulmonary arterioles for seralutinib

4.6mg/kg BID vs vehicle; grade 0=no occlusion, grade 1 partial occlusion and grade 2=complete

occlusion. *(G)* Lumen/media change following seralutinib (4.6 mg/kg) vs vehicle. *(H)*

Representative photomicrograph of IHC staining for pPDGFRβ in seralutinib- (4.6 mg/kg BID) and vehicle-treated animals. Scale bars, 20μm. Arrow indicates increased pPDGFRβ in an occluded small pulmonary artery. Data represent mean ± SEM (for telemetry vehicle n=3, seralutinib n=9 (B); for *C, D, F, G:* vehicle n=8-11*;* seralutinib 2.5mg/kg BID, n=9; seralutinib 4.6mg/kg BID, n=5-6). *$P<0.05$, **$p<0.005$, ***$P<0.001$ and ****$p<0.0001$, seralutinib versus vehicle. Statistical analysis performed by repeated measures analysis of variance (ANOVA) for *B*, ANOVA followed by Dunnett's multiple comparison test versus for *C* and *D*, and unpaired t-test for *F* and *G*. Two animals were not used in the telemetry study due to catheter failures.
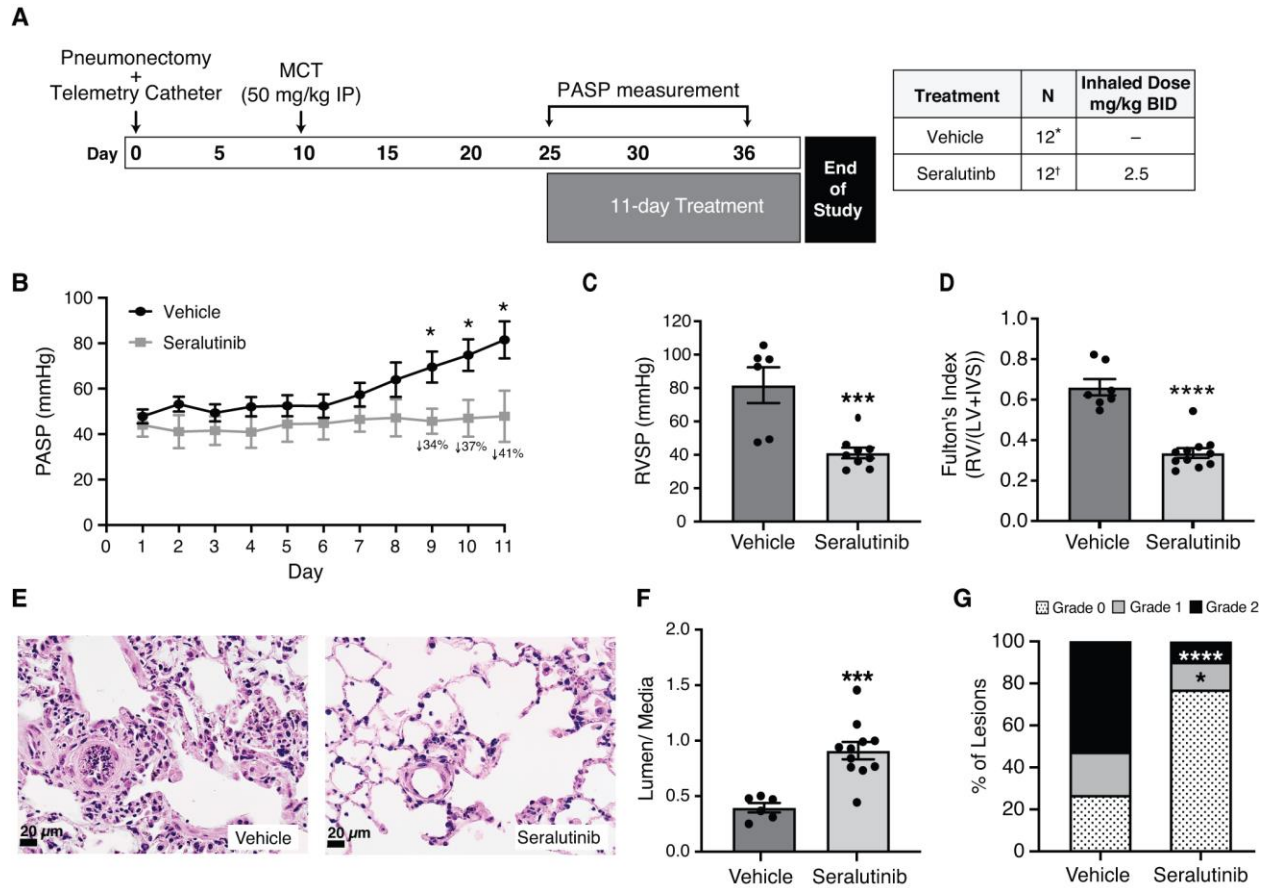
Figure 4. Inhaled seralutinib efficacy in monocrotaline pneumonectomy (MCTPN) model of PAH. *(A)* Study schema for MCTPN model and telemetry study. (*B*) Pulmonary artery systolic pressure (PASP) measured by implanted telemetry device for vehicle (black circle) and seralutinib 2.5mg/kg (grey square) over the course of treatment; *(C)* right ventricular systolic pressure (RVSP), *(D)* right ventricle hypertrophy measured by Fulton's index, *(E)* Representative photomicrograph of immunohistological changes in lung by H & E stain, scale bars, 20μm. *(F)* lumen/media, and *(G)* pulmonary arteriole occlusive grading analysis, where grade 0 = no occlusion, grade 1= partial occlusion and grade 2 = complete occlusion. Data presented as mean ± SEM (vehicle n=11 for *B*, n=6 to 7 for *C-F;* seralutinib 2.5 mg/kg BID, n=

9-11. *$P<0.05$, ***$P<0.001$ and ****$p<0.0001$, seralutinib versus vehicle. Statistical analysis performed by repeated measures analysis of variance for *B*, and unpaired t-test for *C* to *F*.
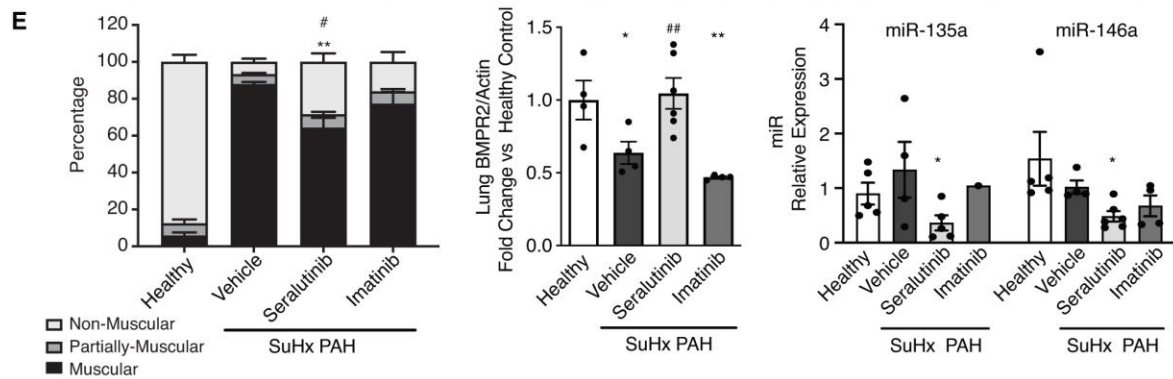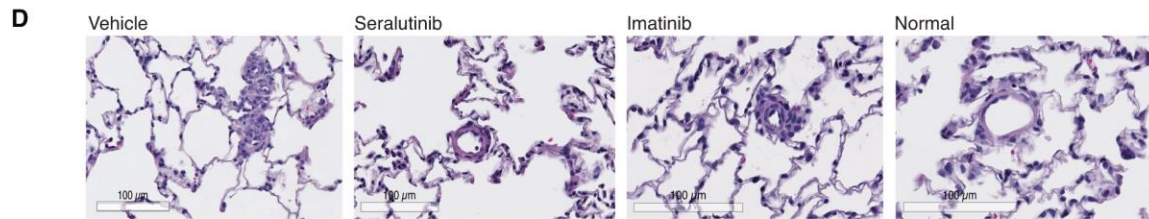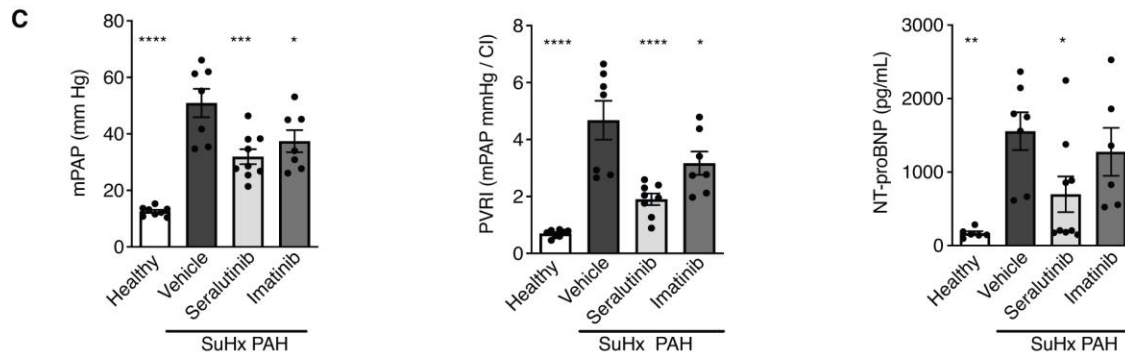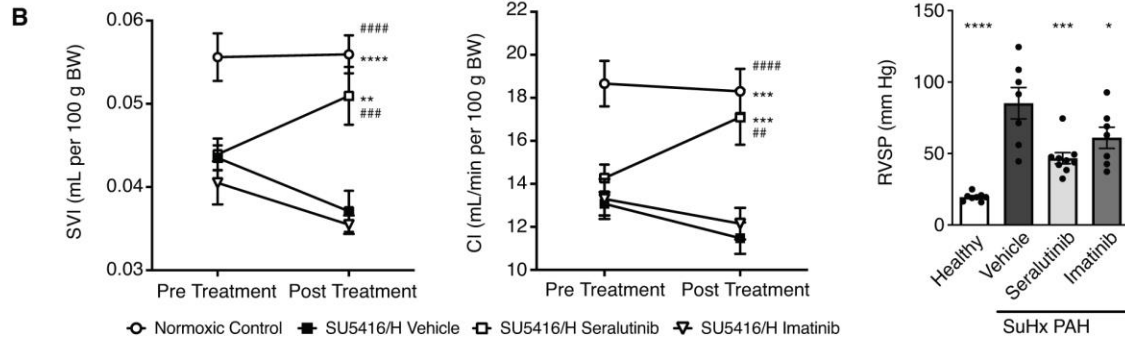
A

SU5416
(20 mg/kg SC)

PAH Induction | PAH Disease Progression

Day | 0 | 7 | 14 | 21 | 28 | 35 | 42 | 49 | End of Study

3-week Hypoxia | 2-week Normoxia | 2-week Treatment

ECHO-based Treatment Group Randomization

ECHO Hemodynamics Tissue Collection

Group	Treatment	N	Dose mg/kg	Route/Regimen
Healthy	–	8	–	–
PAH	Vehicle	8	–	Oral Gavage QD
	Seralutinib	8	12.8	Passive Inhalation BID
	Imatinib	8	15.0	Oral Gavage QD

B

SVI (mL per 100 g BW)

Pre Treatment — Post Treatment

**** ** ###

CI (mL/min per 100 g BW)

Pre Treatment — Post Treatment

*** *** ##

RVSP (mm Hg)

**** *** *

Healthy | Vehicle | Seralutinib | Imatinib
SuHx PAH

○ Normoxic Control ■ SU5416/H Vehicle □ SU5416/H Seralutinib ▽ SU5416/H Imatinib

C

mPAP (mm Hg)

**** *** *

Healthy | Vehicle | Seralutinib | Imatinib
SuHx PAH

PVRI (mPAP mmHg / CI)

**** **** *

Healthy | Vehicle | Seralutinib | Imatinib
SuHx PAH

NT-proBNP (pg/mL)

** *

Healthy | Vehicle | Seralutinib | Imatinib
SuHx PAH

D

Vehicle | Seralutinib | Imatinib | Normal

100 μm | 100 μm | 100 μm | 100 μm

E

Percentage

#
**

Healthy | Vehicle | Seralutinib | Imatinib
SuHx PAH

□ Non-Muscular
▨ Partially-Muscular
■ Muscular

Lung BMPR2/Actin Fold Change vs Healthy Control

* ## **

Healthy | Vehicle | Seralutinib | Imatinib
SuHx PAH

miR Relative Expression

miR-135a | miR-146a

* *

Healthy | Vehicle | Seralutinib | Imatinib   Healthy | Vehicle | Seralutinib | Imatinib
SuHx PAH   SuHx PAH
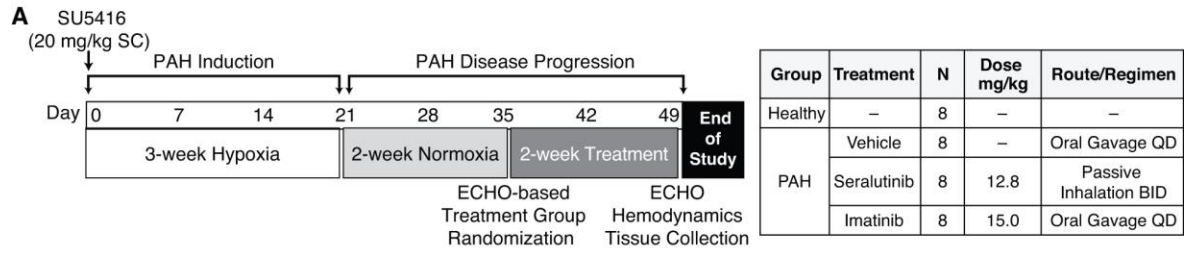
Figure 5. Comparison of inhaled seralutinib and oral imatinib efficacy in SU5416/H model of PAH. (*A*) Study schema for SU5416/H disease induction, progression, and treatment regimen. Echocardiography recording performed on D35 (pre-treatment) and D49 (post-treatment) to measure change in *(B)* stroke volume index (SVI) and cardiac index (CI). Normoxic control (open circle), Vehicle (closed square), inhaled seralutinib (open square) and oral imatinib (open triangle). Bar graphs show hemodynamic parameters (B) RVSP. *(C)* mPAP, PVRI and change in peripheral biomarker of NT-proBNP at the end of treatment (D49). (D*)* Representative photomicrograph of immunohistological changes in lung by H & E stain, scale bars, 100µm *(E)* Change in muscularization, lung BMPR2, miR-135a and miR-146a. Relative miRNA expression is defined as gene expression fold-change relative to the vehicle control group calculated using $2^{\wedge}$-($\Delta\Delta Ct$) values. Data represents mean ± SEM, healthy n=5-8; vehicle n=4-7; seralutinib n=6-9; imatinib n=4-7; n=3 for all groups for change in muscularization. *$P<0.05$, **$p<0.005$, ***$P<0.001$ and ****$p<0.0001$ versus vehicle group; [#]$P<0.05$, [##]$p<0.005$, [###]$P<0.001$ and [####]$p<0.0001$ versus imatinib. Statistical analysis was performed using one-way ANOVA with Dunnett's test for multiple comparisons. Two-way ANOVA with multiple comparison was performed for SVI and CI. One animal was excluded for failure to develop pulmonary hypertension. Statistical analysis of miRNA is described in the Supplement.
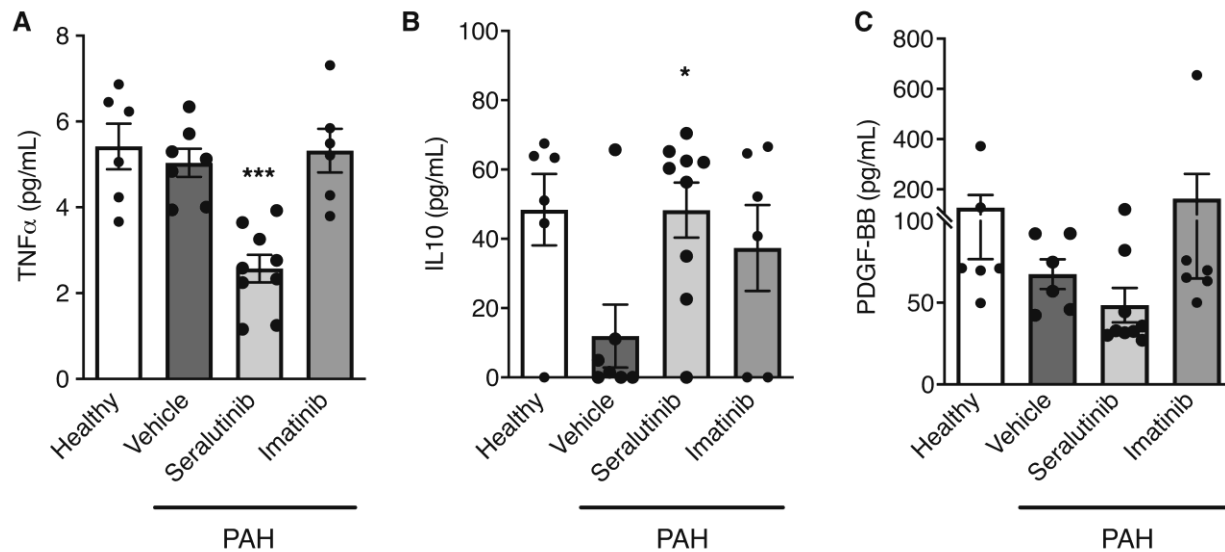
Figure 6. Effect of inhaled seralutinib or oral imatinib on circulating cytokines (*A*) tumor necrosis factor alpha (TNFα), (*B*) interleukin (IL)-10 and (*C*) platelet-derived growth factor (PDGF)-BB at the end of treatment (day 49) in the SU5416/H pulmonary arterial hypertension (PAH) model. Data are shown as mean ± SEM (healthy (n=6), vehicle (n=6–7), seralutinib (n=9), imatinib (n=5–6)). Statistical analysis performed using one-way analysis of variance with Dunnett's multiple comparisons test. *$P<0.05$, ***$P<0.001$ versus vehicle.
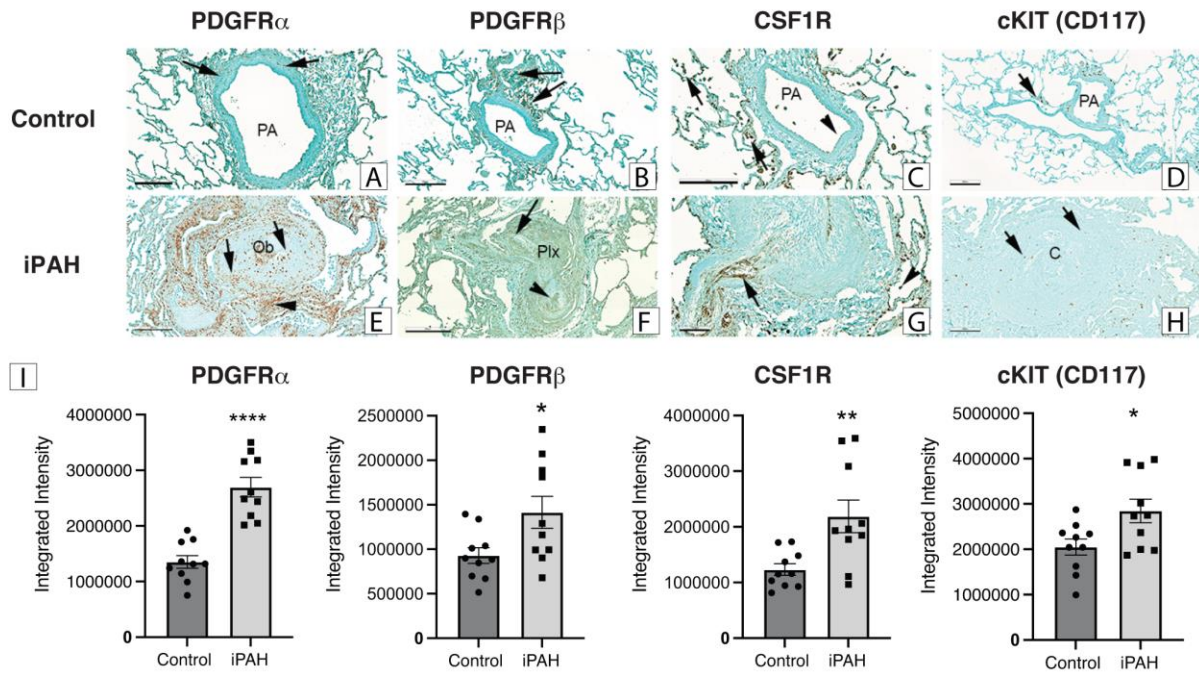
Figure 7. Expression of *(A, E)* PDGFRα, *(B, F)* PDGFRβ, *(C, G)* CSF1R, and *(D, H)* c-KIT in control and iPAH human lungs. *(A)* PDGFRα is expressed in media smooth muscle cells in normal pulmonary arteries (PA) in control lungs (arrows), with (E) marked expression in iPAH obliterative lesion (Ob, arrows) and perivascular tissue (arrowhead). *(B)* PDGFRβ is predominantly expressed in perivascular tissue in control lung (arrows), while *(F)* a complex pulmonary vascular lesion in iPAH shows intense expression in the intima (arrow) and within the incipient blood vessels and cell clusters (Plx, arrow). *(C)* CSF1R expression is noted in the intima of control pulmonary arteries (PA) (arrowhead), with stronger expression in alveolar macrophages (arrows). *(G)* In iPAH lungs, there is marked expression in intima of obliterative lesion (arrow), with expression in macrophages (arrowhead). *(D)* Individual c-KIT positive cells

are sparsely seen around normal pulmonary arteries in control lungs (arrow), while (H) iPAH

lungs show permeation of complex vascular lesions with positive cells (arrows). (Representative

of n=10 control and n=10 iPAH lungs; Scale bars: 100μm (*G*), 200 μm (*A-E, H*), 300 μm (*F*)).

Quantitative analysis demonstrated a significant increase of integrated intensity for PDGFRα,

PDGFRβ, CSF1R and c-KIT, in iPAH lung sections compared to controls (*p<0.05, **p<0.01,
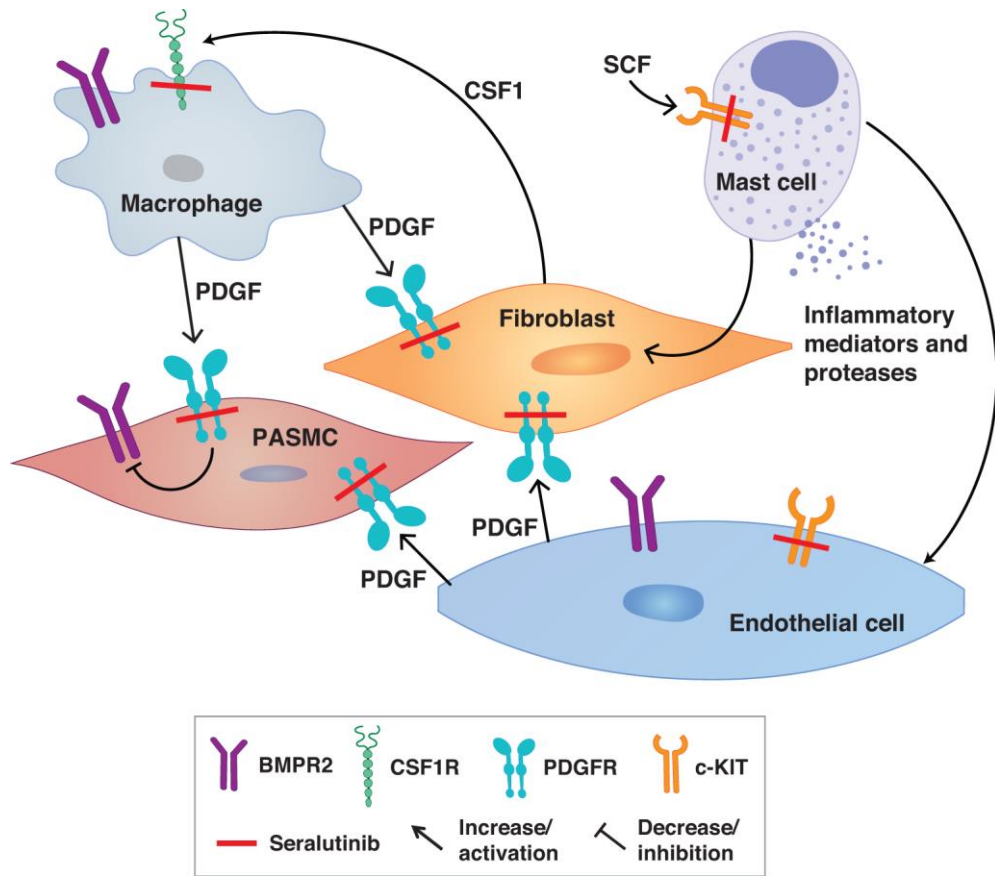
***p<0.0001) (*I*).

Figure 8. Seralutinib inhibits PDGFR, CSF1R, and c-KIT, thereby modulating key signaling pathways involved in pathological remodeling in pulmonary arterial hypertension. Activation of PDGFRs may result in decreased BMPR2 expression. Seralutinib, by inhibiting PDGFR signaling, could increase BMPR2 levels.

Online Supplement

Inhaled Seralutinib Exhibits Potent Efficacy in Multiple Models of Pulmonary Arterial Hypertension

Anna Galkin, Ravikumar Sitapara, Bryan Clemons, Eduardo Garcia, Michael Kennedy, David Guimond, Laura L. Carter, Ashley Douthitt, Robin Osterhout, Aneta Gandjeva, Deborah Slee, Luisa Salter-Cid, Rubin M. Tuder, Lawrence S. Zisman

Methods

Cell Culture

Human cell lines were obtained from commercial vendors and propagated under recommended culture conditions in a humidified incubator at 37°C, with 5% CO_2 in air: NCI-H1703 (ATCC, Manassas, VA, USA), Human Pulmonary Arterial Smooth Muscle Cells (HPASMC, Cell Applications, San Diego, CA, USA), Human Lung Fibroblasts (HLF; Cell Applications, San Diego, CA, USA), HEK-293T (ATCC), and Human Pulmonary Artery Endothelial Cells (HPAECs, Cell Applications, San Diego, CA, USA)

In Vitro **Characterization of Compounds**

Compound activity was assessed in platelet-derived growth factor receptor alpha (PDGFRα), PDGFR beta (PDGFRβ) and colony stimulating factor 1 receptor (CSF1R) enzymatic assays at Carna Biosciences Inc. (Kobe, Japan). A c-KIT enzymatic assay was performed at Gossamer Bio (San Diego, CA, USA) using the Promega c-KIT Kinase Enzyme System (Promega Corporation, Madison, WI, USA). Compounds (starting concentration 1.0E-06M) were titrated in 100% dimethyl sulfoxide (DMSO) then diluted in assay buffer supplements with 50 µM dithiothreitol (DTT) and 2 mM $MnCl_2$. One µL of 5x compound was pre-incubated with 2 µL containing 20 ng of c-KIT protein for 0 and 1 hour in a 384-well low volume plate. The adenosine triphosphate (ATP)/substrate mixture was diluted in assay buffer and 2 µL were added to the compound: enzyme complex with 50 µM final ATP and 1 µg/µL PolyE peptide concentrations as specified by the manufacturer. After two hours at room temperature, 5 µL of adenosine diphosphate (ADP) Glo reagent was added to the plate followed by a 40-minute incubation at room temperature. 10 µL of Kinase Detection Reagent was added and incubated for 30 minutes at room temperature.

Luminescence signal was then measured with the iD5 Spectramax microplate reader (Molecular Devices, Sunnyvale, CA, USA).

H1703 Proliferation Assay

Cells were plated at 1,000 cells/well into a 384-well cell culture plate (Cat#3570, Corning Inc, Poway, CA, USA) and allowed to attach overnight prior to addition of compounds in dose response. Cells were incubated for 72 hours in the presence of treatment and proliferation was assessed by CellTiterGlo Luminescent Cell Viability assay according to manufacturer's directions (Promega Corporation, Madison, WI, USA).[1]

PDGF-BB-Induced Proliferation Assays in HLFs and HPASMCs

HLF cells were plated at a density of 4,000 cells per well in a 96-well cell culture plate (Cat#3904, Corning Inc., Poway, CA, USA) and allowed to attach overnight. Cells were then incubated in 0.1% FBS starvation media (Thermo Fisher Scientific, Waltham, MA, USA) for 24 hours and then compounds were added in dose response. One hour after compound addition, cells were stimulated with 10 ng/ml PDGF-BB (R&D Systems, Minneapolis, MN, USA). Impact on cell proliferation was assessed 48 hours later using CyQuant® Direct Cell Proliferation Assay (Thermo Fisher Scientific, Waltham, MA, USA) according to manufacturer's directions. The values for each concentration are normalized to PDGFB stimulation for day 3 (considered 100% proliferation) and no stimulation for day 3 (0% proliferation).

HPASMC cells were plated at a density of 1,000 cells per well in a Corning® 96-well clear flat bottom polystyrene tissue culture (TC)-Treated plate (Corning Inc., Poway, CA, USA) and attached overnight. One hour after compound addition, cells were stimulated with 25 ng/ml PDGF-BB

(R&D Systems). Impact on cell proliferation was assessed 72 hours later using the CellTiter-Glo®

Luminescent Cell Viability Assay (Promega Corporation, Madison, WI, USA).[1] Day 0 (D0)

represents the basal value at day 0 just prior to PDGFB stimulation.

M-CSF-Induced Activation of CSF1R-SRE Reporter in HEK293 Cells

CSF1R/SRE Reporter Kit (BPS Bioscience, San Diego, CA, USA) was used to assess impact of

compounds of M-CSF-induced CSF1R signaling. HEK-293T cells were seeded at a density of 0.5

million cells per 10-cm plate with complete growth media and incubated for 18 hours until cells

reached 70–90% confluency. HEK293T cells were transfected with the CSF1R expression vector

(~15 µg DNA) and the serum response element (SRE) luciferase reporter construct (~9 µg DNA)

according to the recommended protocol (BPS Bioscience, San Diego, CA, USA). Six hours post-

transfection, cells were re-suspended in growth media with 0.5% FBS, seeded into a 384-well assay

plate (Cat#3570, Corning Inc., Poway, CA, USA) at 10,000 cells per well and allowed to attach

overnight. The following day, cells were pre-incubated with compounds for 30 minutes, prior to

addition of recombinant M-CSF (10 ng/ml final concentration) (BPS Bioscience, San Diego, CA,

USA). Unstimulated control wells received assay medium without CSF1. Cells were incubated for 6

hours prior to lysis and luciferase readout using ONE-Step™ Luciferase Assay System (BPS

Bioscience, San Diego, CA, USA).

Stem Cell Factor (SCF)-Induced Phosphorylation of c-KIT in Human Pulmonary Arterial Endothelial Cells (HPAECs)

HPAECs were plated at a density of 50,000 cells per well in a Corning® 96-well clear flat bottom

polystyrene tissue culture (TC)-Treated plate (Corning Inc., Poway, CA, USA) and attached

overnight. Cells were then incubated in starvation medium (Cell Applications, San Diego, CA,

USA) for 2 hours prior to addition of SCF. Cells were pre-incubated with compound in a 10-point dose response curve for 30 minutes, and then stimulated with 1000 ng/mL SCF (R&D Systems, Minneapolis, MN, USA) for 5 minutes at room temperature. After cell lysis, treatment impact on c-KIT phosphorylation was assessed using the PathScan® Phospho-c-KIT (Tyr719) Sandwich ELISA Kit (Cat# 7298C, Cell Signaling Technologies, Danvers, MA, USA). To detect total c-KIT, the detection antibody provided in the phospho-c-KIT ELISA was replaced with c-Kit Rabbit mAb (clone D3W6Y) at a 1:100 dilution (Cat #37805, Cell Signaling Technologies, Danvers, MA, USA). Data is shown as the percentage of c-KIT phosphorylation over total c-KIT expression.

Extracellular Regulated Kinase (ERK) Signaling Assays

HLF cells were plated at a density of 20,000 cells per well in a Corning® 96-well clear flat bottom polystyrene TC-Treated plate (Corning Inc, Poway, CA, USA), allowed to attach overnight and then incubated in serum-free media for 4 hours prior to addition of compound treatments in dose response. HPASMCs were plated at a density of 10,000 cells per well in a Corning® 96-well clear flat bottom polystyrene TC-Treated plate (Corning Inc, Poway, CA, USA), allowed to attach overnight and then incubated in serum-free media for 2 hours prior to addition of compound treatments in dose response. NCI-H1703 cells were plated at a density of 50,000 cells per well in a Corning® 96-well Clear Round Bottom TC-treated Microplate (Corning Inc, Poway, CA, USA) and allowed to attach for 3 hours prior to addition of compound treatments in dose response. For all cell lines, after a 30-minute compound pre-incubation, cells were stimulated with 25 ng/ml PDGF-BB (R&D Systems, Minneapolis, MN, USA) for 10 minutes. Inhibition of phospho-ERK signal was

then assessed using the advanced phospho-ERK homogeneous time resolved fluorescence (HTRF)

kit (PerkinElmer, Waltham, MA, USA) according to manufacturer's instructions.

Human Macrophage Assays

CD14+ monocytes isolated from human peripheral blood mononuclear cells (PBMCs) (StemExpress, San Diego, CA, USA) were seeded into 6-well tissue culture plates at a density of 500,000 cells per well in Differentiation Media (RPMI-1640, 1x Gentamicin, 1x non-essential amino acids (NEAA) and 10% heat inactivated FBS (Thermo Fisher Scientific) supplemented fresh with 10 ng/ml macrophage CSF (M-CSF) (PeproTech, Rocky Hill, NJ, USA). Media was replenished every 3–4 days. On day 8, Differentiation Media was further supplemented with 20 ng/ml recombinant human interleukin (IL)-4 and 20 ng/ml recombinant human IL-13 (PeproTech, Rocky Hill, NJ, USA) and cells were incubated for 24 hours prior to conditioned media collection for assessment of human monocyte chemoattractant protein-1 (MCP-1/CCL2) secretion using the MCP1 HTRF kit (Cisbio, Bedford, MA, USA).

To evaluate impact of seralutinib and imatinib on CSF1R phosphorylation in primary macrophages, monocytes were allowed to attach and differentiate into macrophages using Differentiation Media as described above. On day 8 of culture, cells were serum starved with compound for 2 hours, and stimulated with recombinant human M-CSF (50 ng/ml) (PeproTech, Rocky Hill, NJ, USA) for 5 minutes prior to lysis. Treatment impact on CSF1R phosphorylation was assessed using the PathScan® Phospho-M-CSF Receptor (panTyr) and the PathScan® Total M-CSF Receptor Sandwich ELISA Kits (Cell Signaling Technologies, Danvers, MA, USA).

Inhaled Delivery of Seralutinib

Seralutinib was formulated as a dry powder with aerosol properties designed to allow deposition in the deep lung. Placebo consisted of excipient without active ingredient. CH Technologies (Westwood, NJ, USA) system designed for passive inhalation drug delivery in rats with either a Rotating Brush Generator or Vilnius Dry Powder Generator was used for dosing.

Pharmacokinetic (PK) and Pharmacodynamic (PD) Assessments

To understand dose- and time-dependent PK/PD effects of seralutinib treatment compared to placebo, seralutinib was administered for 4 days via passive inhalation (120-minute treatment per day) at three dose levels: low (4.3 mg/kg/dose), mid (16.2 mg/kg/dose), and high (66.6 mg/kg/dose) to healthy 8–9-week-old Sprague Dawley male rats. Delivered dose levels were estimated using Alexander's formula.[2]

Immediately post-inhalation, a subset of animals were anesthetized and treated with either 300 µg rat PDGF-BB (GenScript Biotech, Nanjing, China) (PD study 1) or a cocktail of 150 µg rat PDGF-BB + 50 µg rat SCF (PeproTech, Rocky Hill, NJ, USA) (PD Study 2) reconstituted in 200 µl 0.1% bovine serum albumin (BSA) (prepared in sterile 0.9% NaCl) and delivered via pulmonary insufflation using a Penn-Century® Microsprayer (Penn-Century, Wyndmoor, PA, USA) 5 minutes prior to lung tissue collection to facilitate detection of PDGFR and cKIT autophosphorylation.

Rat lung lobes and plasma samples were collected for bioanalysis immediately at the end of inhalation dosing, 4, 8, 16, and 24 hours from the start of treatment and frozen in liquid nitrogen.

Seralutinib plasma and lung homogenate concentrations were determined against standard curves of known concentration using a protein precipitation extraction followed by separation and detection by liquid chromatography tandem mass spectrometry (LC-MS/MS).

Lung Tissue Protein and Messenger RNA (mRNA) Extraction Procedures

To generate lung protein lysates, approximately 100 mg of the left lung lobe was weighed and placed in a centrifuge tube containing 2 mm zirconia beads (BioSpec Products, Bartlesville, OK, USA) and 1 ml of RIPA Lysis Buffer with phosphatase and protease inhibitors (Thermo Fisher Scientific, Waltham, MA, USA). Samples were then placed in a Mini-Beadbeater-96 (BioSpec Products, Bartlesville, OK, USA) and homogenized for 2 minutes at 2,500 rpm. The samples were cooled on ice for 10 minutes, and then centrifuged at 20,000 x g for 10 minutes. Lysate was pipetted into clean centrifuge tubes, while carefully avoiding the pelleted debris. The Rapid Gold BCA Protein Assay (Thermo Fisher Scientific, Waltham, MA, USA) was performed to quantify the protein concentration of each sample, and then diluted accordingly in Lysis Buffer to normalize each sample concentration to 10 mg/ml. Samples were stored at –80°C.

To extract lung tissue RNA, approximately 20–30 mg of lung tissue from the right upper lobe was disrupted and homogenized in Buffer RLT using the TissueLyser II (QIAGEN, Hilden, Germany). Lysates were processed on the QiaCube Connect using the QIAGEN RNeasy Mini Kit following the manufacturer's instructions, including the optional DNase I treatment (QIAGEN, Hilden, Germany). RNA was quantified using a NanoDrop 2000 (Thermo Fisher Scientific, Waltham, MA, USA), assessed for RNA integrity and quality using the Qubit 4 Fluorometer (Thermo Fisher Scientific, Waltham, MA, USA) and converted into complementary DNA (cDNA) using the High-Capacity Reverse Transcription Kit (Thermo Fisher Scientific, Waltham, MA, USA).

Quantitative Polymerase Chain Reaction (qPCR) Methods

MCP-1 (CCL2, Rn00580555_m1) and housekeeping control ACTB (Rn00667869_m1) mRNA expression levels were detected using the TaqMan™ Universal PCR Master Mix (no AmpErase™ UNG; Thermo Fisher Scientific, Waltham, MA, USA) on the QuantStudio5 (Thermo Fisher Scientific, Waltham, MA, USA). Data were analyzed using the QuantStudio Design & Analysis Software (Thermo Fisher Scientific, Waltham, MA, USA), with Ct thresholds being set in the linear range. Fold changes were calculated using the delta Ct ($\Delta\Delta$Ct) method, where Ct values were first normalized to ACTB, and then to the untreated control.

Assessment of Lung Protein Expression

Traditional Western blot analysis was performed to measure levels of phopsho-PDGFRβ Tyr1021, phospho-PDGFRα/β (Tyr849)/(Tyr857), total PDGFRβ, phospho-cKIT Tyr719 and β-actin. The following antibodies were used for protein expression: pPDGFRβ Y1021 at 1:500 (Cat# 2227), pPDGFRα/β (Tyr849)/(Tyr857) at 1:500 (Cat#3170), total PDGFRβ at 1:1,000 (Cat# 3169), phospho-cKIT Tyr719 at 1:500 (Cat# 3391) and β-Actin at 1:2,000 (Cat# 4970) (all from Cell Signaling Technologies, Danvers, MA, USA); total cKIT Ab at 1:500 (Cat# LS-C382844) from Lifespan Biosciences (Seattle, WA, USA). The immunoreactive bands were quantified by densitometry. Expression of phospho-proteins was normalized to respective total protein. Data are presented as percentage inhibition relative to control untreated samples.

The WES instrument (ProteinSimple, San Jose, CA, USA) was used to quantitate bone morphogenetic protein receptor type 2 (BMPR2) and phospho-SMAD1/5 protein level expression in rat lung lysates using the following antibodies: Anti-BMPR-II (RUO), Clone 18 (Cat# 612292, BD Biosciences), phospho-Smad1/5 (Ser463/465) (41D10) (Cat#9516, Cell Signaling

Technologies, Danvers, MA, USA) and β-actin (13E5) Mouse mAb (Cat #3700, Cell Signaling Technologies, Danvers, MA, USA). Area under the curve was calculated for each protein of interest and normalized to expression of β-actin. Data are shown as fold induction relative to control.

Rat Models of Pulmonary Arterial Hypertension (PAH)

For the monocrotaline pneumonectomy (MCTPN) model (Study 1) and the SU5416/H studies (Study 2 and 3) Guyton's formula[3] was used to estimate minute ventilation which was then used to estimate the average delivered dose for the animals.

SU5416/H Model (Study 1)

The purpose of this preclinical efficacy study was to determine efficacy of seralutinib when delivered as a dry powder in the rat SUGEN5416/hypoxia/normoxia model. Two cohorts were studied. Cohort 1 consisted of eight vehicle-treated animals and nine seralutinib-treated animals. Three of the vehicle animals had telemetry monitoring and all nine of the seralutinib-treated animals in cohort 1 had telemetry monitoring. In the telemetry subset of cohort 1, male Sprague Dawley rats underwent placement of DSI PAC40 telemetry devices (Data Sciences International) with catheter tip in the main pulmonary artery. After 10 days' recovery, the animals were administered SUGEN5416 (Sigma-Aldrich, St Louis, MO, USA) 20 mg/kg subcutaneous (SC) in carboxymethylcellulose/dimethyl sulfoxide (CMC/DMSO) suspension and placed in a COY hypoxia chamber with fraction of inspired oxygen (FiO_2) 10% (Cor Laboratory Products Inc, Grass Lake, MI, USA). The animals resided in the hypoxia chamber for 3 weeks. They were removed once a week for less than 10 minutes to monitor pulmonary artery (PA) pressures. After week 3 (day 21) they were removed from the hypoxia chamber permanently and PA pressures were monitored continuously for the first 24 hours. They were allowed to equilibrate to normoxia, and on

day 2 after removal from the chamber were assigned to inhaled placebo or inhaled seralutinib 2.5 mg/kg twice daily.

Cohort 2 consisted of six vehicle-treated rats and six rats treated with inhaled seralutinib. Rats were administered SU5416 20 mg/kg SC and placed in the hypoxia chamber for 3 weeks at 10% FiO_2. Treatment was started on day 2 after removal from hypoxia. In the cohort 2 active group, the average dose of seralutinib was 4.6 mg/kg twice daily. This cohort underwent end of study measurement of RV pressure, lumen/media analysis, and occlusive grading analysis of pulmonary arterioles.

Hemodynamics

Telemetry monitoring was recorded for 10 minutes of each hour for the study period. During dosing itself telemetry was not recorded due to logistical constraints of the telemetry system. RV pressure was also determined at the end of study.

End of Study Procedures

End of study procedures consisted of placement of a Scisense catheter (Transonic Systems) in the right ventricle for recording of RV hemodynamics. At the end of the study, the right upper or middle lobe of the lung was tied off, removed, and placed in liquid nitrogen. Then the heart and remaining lung were removed en bloc. The heart chambers (LV, IVS, RV) were dissected and weighed. The lung PA was perfused with heparinized saline then 10% formalin. 10% formalin was also used to inflate the lung via the trachea. The lung lobe snap frozen in liquid nitrogen was placed at minus 80°C for storage. After 2 days the formalin-infused organs were switched to 70% histology grade alcohol.

Histology and Morphometric Analysis

In cohort 2, H&E-stained sections of the lung were analyzed for pulmonary arteriole lumen/media ratio and grading of plexiform lesions. Sections were imaged with a standard bright field microscope with 10X and 40X objectives, and photomicrographs analyzed with ImageJ software (NIH, Bethesda, MD, USA). In one case lumen/media ratio was not determined. Immunohistochemistry was performed with a phospho-specific antibody against the PDGFRβ receptor (SC-12909) (Santa Cruz Biotechnologies, Dallas, TX, USA).

MCTPN Model (Study 2)

Telemetry

Study rats underwent implantation of a pulmonary artery (PA) monitoring telemetry catheter (DSI PAC40, Data Sciences International, St Paul, MN, USA) and left pneumonectomy with the exception of two animals in the seralutinib group which only underwent left pneumonectomy. Ten days after recovering from surgery all the pneumonectomized rats were given monocrotaline (Sigma-Aldrich, St. Louis, MO, USA) 50 mg/kg intraperitoneal (IP). Dosing of vehicle started, on average, 16 days after monocrotaline administration. Dosing of seralutinib started, on average, 20 days after monocrotaline administration. Seralutinib (2.5 mg/kg) dry powder or vehicle was administered by nose only inhalation 30 minutes (on average) twice daily to the rats via a Vilnius Dry Powder Generator (CH Technologies) connected to the Exposure tower (CH Technologies) for 11 days.

There were 12 animals in the vehicle group and 12 animals in the seralutinib-treated group. Pulmonary hypertension did not develop in one animal in the seralutinib group, and this animal was

excluded from the analysis. The DSI PAC40 malfunctioned in two other animals in the seralutinib group, and the telemetry data were not used from these two animals in the analysis. In the vehicle group, after 11 days of being administered vehicle, five of the animals were crossed over to seralutinib treatment and treatment was continued in these animals for up to 9 days. In the cross-over extension study, most of the animals in the vehicle group and some of the animals crossed over from vehicle to seralutinib required early euthanasia for distress. Data from end of study procedures, including measurement of right ventricular pressure, lumen to media ratio and heart weights for the vehicle group are reported for the vehicle animals that were not crossed over to seralutinib treatment and the primary seralutinib-treated group.

Plethysmography

Two chamber plethysmography was measured at end of study using an EMKA system and IOX software (EMKA Technologies, Montreal, Canada). Measurements included tidal volume, respiratory rate, minute ventilation, and airway resistance.

End of Study Procedures

At the end of the study rats underwent general anesthesia, intubation, left thoracotomy, and insertion of a Scisense catheter (Transonic Systems, Ithaca, NY, USA) to measure right ventricular pressures directly. The animals were heparinized, then euthanized by exsanguination under general anesthesia, and the heart and lungs excised. The pulmonary artery was perfused with heparinized saline followed by formalin, and the lung infused with 10% formalin via the trachea for a total volume of 1.5 ml. The heart was dissected, and the right ventricular free wall (RV), interventricular septum (IVS), and left ventricle (LV) were weighed separately. The ratio RV/(IVS+LV) was determined to evaluate right ventricular hypertrophy (RVH).

Measurement of Pulmonary Arteriole Lumen to Media Ratio

The lumen to media area ratio was determined on pulmonary arterioles from hematoxylin and eosin (H&E)-stained lung sections. Areas were traced with Image J software and pixel areas determined. The pulmonary arteriole media area was determined by subtracting the lumen area from the total vessel area encompassed by the outer media circumference. Taking the ratio of the lumen to media helps normalize for differences in blood vessel size. A vehicle-treated animal was found dead on the last day of dosing. The lungs were hemorrhagic and were not used for lumen/media analysis.

Grading of Neointimal Proliferation

Based on the method of Toba et al,[4] neointimal proliferation was graded according to the following system: Grade 0 (no significant obstruction), Grade 1 (<50% obstruction), Grade 2 (>50% obstruction of the vessel lumen). Picrosirius Red staining was performed to evaluate the extent of fibrosis.

SU5416/H Model (Study 3)

The purpose of this study was to directly compare efficacy of inhaled seralutinib to orally administered imatinib in the SU5416/H model. The model was developed as in Study 2 with a single injection of SU5416 20 mg/kg (AdooQ Bioscience, Irvine, CA, USA) followed by three weeks of hypoxia. In this study, echocardiography was performed to assure equal disease severity distribution between the treatment groups at the start of treatment and to assess the effect of treatment on cardiac performance non-invasively.

Echocardiography to monitor disease progression was carried out on days 0, 35, and 49. An echocardiograph (Model Q9, Chison Medical Imaging Co., Jiangsu, China) connected to a Chison

12.0 MHz probe was used to measure the pulmonary artery maximum velocity (Vmax), the Artery Pulmonary Velocity Time Integral (VTI), the pulmonary artery diameter, and heart rate. Randomization into treatment groups on day 35 was based on the following parameters: cardiac output (CO), pulmonary artery Vmax, and stroke volume (SV).

Treatment with inhaled seralutinib, oral gavage imatinib, or oral gavage vehicle control (40% PEG 300/60% Acetic Acid-acetate Buffer pH 4.6) was initiated on day 35, 2 weeks after animals were returned to normoxia. Seralutinib was administered twice daily by inhalation (60 minutes) at an estimated dose of 12.8 mg/kg/dose using a Vilnius Aerosol Generator connected to an inhalation tower (CH Technologies). Mercer-style cascade impactor (CH Technologies, Westwood, NJ, USA) was used to perform aerodynamic particle size distribution measurements. Imatinib 15 mg/kg was administered by oral gavage once a day. A set of healthy control rats were also included in the study. The selected dose was consistent with prior published studies, which evaluated imatinib doses of 5 to 50 mg/kg in rat PAH models.[5-7] Furthermore, imatinib activity was confirmed in the phospho-PDGFR rat PD model, demonstrating potent inhibition of PDGFR phosphorylation (**Figure S4**).

End of Study Procedures

On day 49, after 2 weeks of treatment, end of study procedures were performed: mean pulmonary arterial pressure (mPAP) and right ventricle systolic pressure (RVSP) were measured via an intra-arterial fluid-filled catheter (AD Instruments, Colorado Springs, CO, USA). Pulmonary vascular resistance index (PVRI) was calculated using the following formula: PVRI = mPAP / CI, where mPAP is mean pulmonary arterial pressure (mm Hg) and CI is cardiac index, defined as Cardiac

Output (ml/min) normalized to 100 g body weight. Stroke Volume Index (SVI) was defined as SV normalized to 100g body weight.

At the end of the hemodynamic measurements, right middle lung lobes were tied off with suture, excised, and snap frozen in liquid nitrogen for bioanalysis. The rest of the lung tissue was perfused with 10% formalin for histopathology analysis.

Plasma samples were collected at study termination for biomarker follow up. Circulating levels of NT-proBNP were assessed with the Rat NT-proBNP sandwich immunoassay kit (#K153JKD) as per manufacturer's protocol (Meso Scale Discovery, Rockville, MD, USA). Rat Pro-Inflammatory Panel 2 immunoassay kit (#K15059D, Meso Scale Discovery) and mouse/rat PDGF-BB Quantikine ELISA (MBB00, R&D Systems) were used to assess circulating plasma cytokines and PDGF-BB respectively. MCP-1 (CCL2) expression was determined using the Rat MCP-1 Ultrasensitive immunoassay kit (#K153AYC) as per manufacturer's protocol (Meso Scale Discovery).

Histopathology Methods

Left lung lobes were harvested, perfused, and fixed with 10% formalin before being sent to the Institute for Research in Immunology and Cancer in Montreal, Quebec, Canada, for embedding, sectioning, and staining with H&E. Scanned images were then analyzed by a blinded histopathologist. Fifty intra-acinar vessels associated with alveoli, alveolar ducts and respiratory bronchioles were analyzed. All vessels associated with terminal bronchioles and all larger airways were excluded. Each vessel was categorized as non-muscular (single elastic lamina for all of circumference), semi-muscular (10–90% smooth muscle layer circumference) or muscular (>90% smooth muscle layer circumference). NDP view 2.7.25 Zoomer Digital Pathology (Hamamatsu Photonics, Hamamatsu City, Japan) software was used for the analysis. A complementary analysis

of the small pulmonary arteries was performed using lung sections stained with α-smooth muscle actin (SMA; # M0851, Agilient, Santa Clara, CA): 30-50 Small vessels less than 100 microns and plexiform lesions where present were analyzed per sample using Aperio Imagescope software. Average Signal intensity was normalized to area analyzed. ANOVA followed by the Bonferroni correction was used for statistical analysis.

Rat microRNA analysis

miRNA Extraction

Ten to twenty mg of lung tissue from the right upper lobe (from SU5416 Study 3) were weighed and kept on dry ice in a 2.0 mL Eppendorf tube. As a recommended control, a master mix of 1 µL of RNA-Spike mix containing UniSp2, UniSp4, and UniSp5 was added for every 700 µL of QIAzol as a QC control. Immediately prior to lysing, one 5 mm stainless steel bead and 701 µL of QIAzol mix was added to each tube. The tubes were loaded onto the TissueLyser II and were homogenized for 2 minutes at 25.0 Hz. Once complete, the extraction followed the manufacturer's protocol by using the miRNeasy Mini Kit Protocol for animal tissue found on the QIAcube Connect. miRNA samples were then quantified by the NanoDrop2000. Leftover RNA was frozen in the -80 for long-term storage.

cDNA Preparation

The cDNA reaction was prepared using the miRCURY LNA RT Kit (QIAGEN, Hilden, Germany). UniSp6 was reconstituted in combination with cel-miR-39-3p as an additional spike-in control for the reverse transcription process. Twenty ng of template RNA was added to the reaction mix as per the manufacturer's protocol, and was prepared using the conditions described with the miRNome PCR Mouse/Rat Panel I.

qPCR Assay

miRCURY LNA miRNome Mouse/Rat PCR Panels intended for use with QuantStudio PCR Systems (Catalog # YAMR-301YE-4) were purchased from QIAGEN (Hilden, Germany). Prior to each run, one plate was thawed and spun down to pellet lyophilized primer pellets. The miRCURY LNA SYBR Green PCR Kit (Catalog# 339347) was purchased for use to prepare samples for qPCR assays. Master mix was prepared following the manufacturer's protocol with the low ROX dye concentration due to the thermal cycler being used. Plates were sealed, briefly vortexed, then spun down prior to loading on the instrument. The PCR cycling conditions used followed the protocol, with a 2-minute inactivation at 95°C, followed by 40 cycles of 10 second denaturation at 95°C and 60 second annealing/extension at 56°C. A melt curve was performed after the PCR as a QC check.

Data Analysis

Data was first analyzed by using Thermo Fisher's QuantStudio Design & Analysis software to ensure all thresholds were consistent across all different plates to produce Ct values. The Ct values were then normalized to ΔCt values using inter-plate calibrators followed by geNorm normalization as described by Vandesompele.[8] miRNA families predicted to target rat and human BMPR2 were downloaded from TargetScan (release 8.0).[9] Only miRNA predicted to target both rat and human BMPR2 were retained for differential expression analysis. P-values for pairwise comparisons among treatment groups were calculated using the limma eBayes method (version 3.46)[10] in R (version 4.1.2). miRNA with a p-value below 0.05 and absolute ΔΔCt change greater than or equal to 1 were considered differentially expressed. Fold change values for between-group comparisons are derived from the ΔΔCt values, using the formula 2^(-ΔΔCt).

Immunohistochemistry of PAH lung explants and control lungs

Human lung samples for immunohistochemistry were obtained from the PHBI tissue repository as formalin fixed paraffin embedded specimens. Control samples consisted of donor lungs not used for transplant. Ten PAH and ten controls samples were studied. The clinical data is shown in **Table S3**. Antigen retrieval was performed with citrate solution (Vector Laboratories). Sections of formalin-fixed paraffin-embedded (FFPE) lung tissues were stained with the following primary antibodies: PDGF Receptor α (3174; 1;100, Cell Signaling Technologies, Danvers, MA, USA), PDGF Receptor β (3169; 1:100; Cell Signaling Technologies, Danvers, MA, USA), CD117 (NCL-L-CD117-032, pre-diluted, Leica Biosystem, Nussloch, Germany), CSF1R, (OAAB18690; 1:500, Aviva Systems Biology, San Diego, CA, USA).

Antibody binding was visualized with DAKO polymer labeled, HRP-bound, secondary reagent (DAKO Envision+ HRP rabbit (K4010) and HRP mouse (K4006). For counterstain, Light Green (STLGCPT-StatLab Medical Products) was used. The slides were scanned by the Aperio system (Leica Biosystems, Buffalo Grove, IL) and visualized in its ImageScope software. Random images focused on pulmonary arteries were captured at 10x magnification as jpeg files and coded for masked analyses. Coded images were uploaded into Metamorph (Molecular Devices, San Jose, CA), thresholded based on positive control immunohistochemical signal and the signal quantified using the region measurement application of the image software. This approach was used in our prior publications.[11-13]

Anti-PDGFRα, PDGFRβ and CSF1R antibodies described above were rat-cross reactive and were used for staining FFPE lung tissues from both the MCTPN and SU5416/H rats treated with vehicle or seralutinib. The c-KIT antibody was not cross-reactive, and therefore c-KIT staining was not evaluated in rat tissues.

Statistical Analysis

Data are presented as mean ± standard error of the mean (SEM) unless otherwise indicated. Statistical analysis was performed with XLSTAT (Addinsoft, Paris, France) or GraphPad Prism (GraphPad, La Jolla, CA, USA). For all studies, significance was set at $P<0.05$. For monocrotaline pneumonectomy model (MCTPN) Study 2 data, the unpaired t-test was used to compare pulmonary artery pressures, lumen to media ratio, respiratory parameters, and right ventricular hypertrophy (RVH), between the vehicle and seralutinib-treated groups. Analysis of neointimal proliferation grade was performed with the Mann-Whitney test. For the SU5416/H Study 1 analysis of variance (ANOVA) or repeated measures ANOVA was performed with the Bonferroni correction for multiple group comparisons. The unpaired t-test was used for 2 group comparisons. The Kruskal Wallis test was used for the graded occlusive lesion analysis. SU5416/H Study 3 statistics were calculated using a one-way ANOVA with Dunnett's or Tukey's Multiple Comparisons Test.

References

1.   McDermott U, Ames RY, Iafrate AJ, et al. Ligand-dependent platelet-derived growth factor receptor (PDGFR)-alpha activation sensitizes rare lung cancer and sarcoma cells to PDGFR kinase inhibitors. *Cancer Res* 2009; 69: 3937-3946. 2009/04/16. DOI: 10.1158/0008-5472.CAN-08-4327.

2.   Alexander DJ, Collins CJ, Coombs DW, et al. Association of Inhalation Toxicologists (AIT) working party recommendation for standard delivered dose calculation and expression in non-clinical aerosol inhalation toxicology studies with pharmaceuticals. *Inhal Toxicol* 2008; 20: 1179-1189. 2008/09/20. DOI: 10.1080/08958370802207318.

3.   Guyton AC. Measurement of the respiratory volumes of laboratory animals. *Am J Physiol* 1947; 150: 70-77. 1947/07/01. DOI: 10.1152/ajplegacy.1947.150.1.70.

4.   Toba M, Alzoubi A, O'Neill KD, et al. Temporal hemodynamic and histological progression in Sugen5416/hypoxia/normoxia-exposed pulmonary arterial hypertensive rats. *Am J Physiol Heart Circ Physiol* 2014; 306: H243-250. 2013/11/19. DOI: 10.1152/ajpheart.00728.2013.

5.   Leong ZP, Okida A, Higuchi M, et al. Reversal effects of low-dose imatinib compared with sunitinib on monocrotaline-induced pulmonary and right ventricular remodeling in rats. *Vascul Pharmacol* 2018; 100: 41-50. 2017/11/05. DOI: 10.1016/j.vph.2017.10.006.

6.   Sakao S, Tatsumi K and Voelkel NF. Reversible or irreversible remodeling in pulmonary arterial hypertension. *Am J Respir Cell Mol Biol* 2010; 43: 629-634. 2009/12/17. DOI: 10.1165/rcmb.2009-0389TR.

7.   Schermuly RT, Dony E, Ghofrani HA, et al. Reversal of experimental pulmonary hypertension by PDGF inhibition. *J Clin Invest* 2005; 115: 2811-2821. 2005/10/04. DOI: 10.1172/JCI24838.

8.   Vandesompele J, De Preter K, Pattyn F, et al. Accurate normalization of real-time quantitative RT-PCR data by geometric averaging of multiple internal control genes. *Genome Biol* 2002; 3: RESEARCH0034. 2002/08/20. DOI: 10.1186/gb-2002-3-7-research0034.

9.   Agarwal V, Bell GW, Nam JW, et al. Predicting effective microRNA target sites in mammalian mRNAs. *Elife* 2015; 4 2015/08/13. DOI: 10.7554/eLife.05005.

10.   Ritchie ME, Phipson B, Wu D, et al. limma powers differential expression analyses for RNA-sequencing and microarray studies. *Nucleic Acids Res* 2015; 43: e47. 2015/01/22. DOI: 10.1093/nar/gkv007.

11.   Petrache I, Natarajan V, Zhen L, et al. Ceramide upregulation causes pulmonary cell apoptosis and emphysema-like disease in mice. *Nat Med* 2005; 11: 491-498.

12.   Schmidt EP, Yang Y, Janssen WJ, et al. The pulmonary endothelial glycocalyx regulates neutrophil adhesion and lung injury during experimental sepsis. *Nat Med* 2012; 18: 1217-1223. DOI: nm.2843 [pii];10.1038/nm.2843 [doi].

13.   Yoshida T, Mett I, Bhunia AK, et al. Rtp801, a suppressor of mTOR signaling, is an essential mediator of cigarette smoke-induced pulmonary injury and emphysema. *Nat Med* 2010; 16: 767-773. DOI: nm.2157 [pii];10.1038/nm.2157 [doi].

Table S1. Seralutinib *In* Vitro Potency Versus Imatinib

Compound	Biochemical IC$_{50}$ (nM)				Cell-Based IC$_{50}$ (nM)							
	PDGFRα*	PDGFRβ*	CSF1R*	c-KIT[†]	H1703 (PDGFRα)[‡]	HLF (PDGFRβ >α)[§]	HPASMC (PDGFR α=β)[ll]	H1703 pERK**	HLF pERK**	[††]CSF1R pCSF1R	[†††]CSF1R Reporter assay	HPAECs pc-KIT[‡‡]
Seralutinib	7	14	92	20	32	29	33	70	60	14.4	8	7.8
Imatinib	8	75	1160	180	62	579	419	260	>10,000	500	1032	301

CSF1R = colony stimulating factor 1 receptor; HLF = human lung fibroblast; HPASMC = human pulmonary arterial smooth muscle cell; HPAEC = human pulmonary artery endothelial cells; PDGFR = Platelet-derived growth factor receptor; SCF = stem cell factor, M-CSF1= macrophage colony stimulating factor.
*Carna biochemical assay.
[†]c-KIT biochemical assay.
[‡]H1703 proliferation assay.
[§]PDGF-BB-induced HLF proliferation assay.
[ll]PDGF-BB-induced HPASMC proliferation assay.
**PDGF-BB induced pERK signaling assay in H1703 and HLF cells.
[††]M-CSF-induced pCSF1R in primary human macrophages.
[†††]M-CSF-induced activation of CSF1R-SRE reporter in HEK293.
[‡‡]SCF-induced phosphorylation of wild type KIT in HPAECs
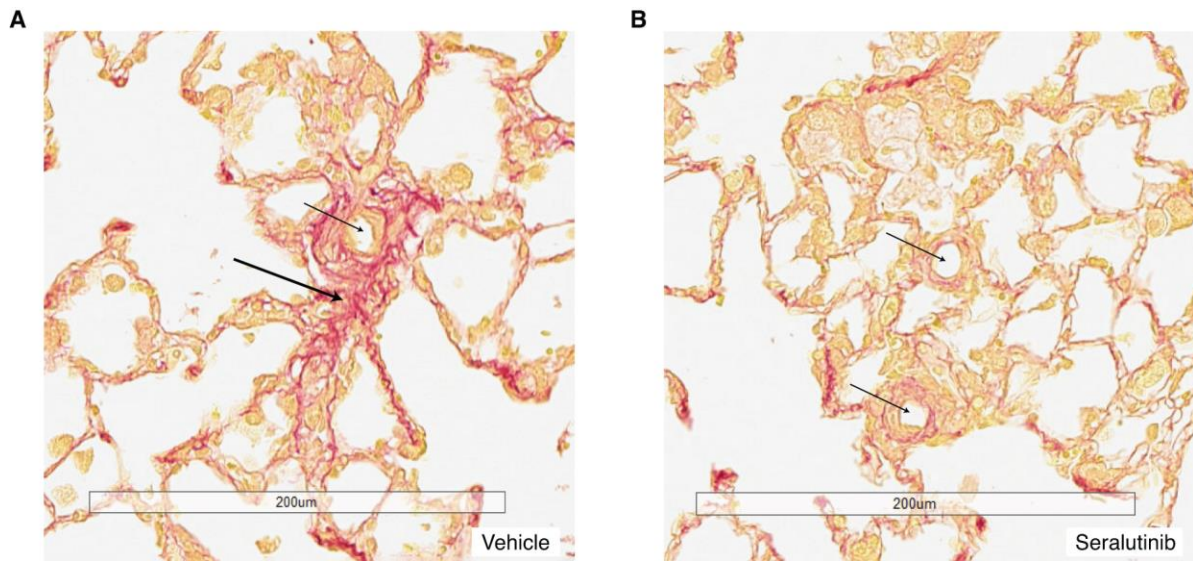
Figure legends

Figure S1. Immunohistology for fibrosis in lungs from MCTPN study using Picrosirius Red Stain. Representative photomicrograph of Picrosirius stain in vehicle (*A*) and seralutinib-treated group (*B*). Thin arrows point to pulmonary arteriole lumen. (*A*) Vehicle-treated animal showing extensive peri-vascular fibrosis (thick arrow). (*B*) Seralutinib-treated animal. Scale bars, 200μm.
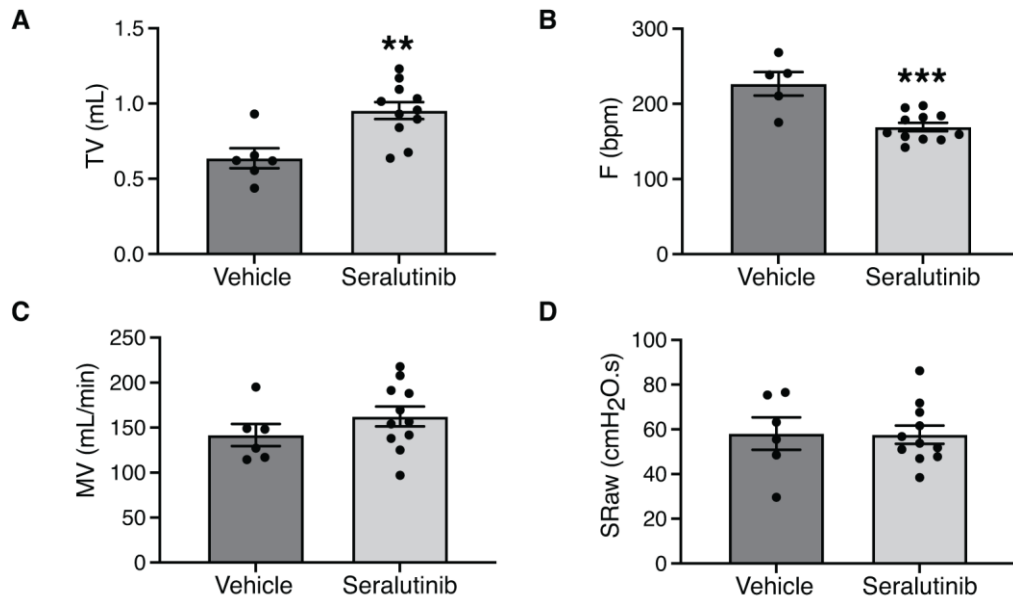
Figure S2. Effects of seralutinib on respiratory parameters in the monocrotaline pneumonectomy (MCTPN) model. Bar graphs shows effect of seralutinib (light grey) vs vehicle (dark grey) on (*A*) tidal volume (TV), (*B*) respiratory rate (F; bpm, breaths per minute), (*C*) minute ventilation (MV; milliliters per minute), and (*D*) airway resistance (Sraw; cmH$_2$O.s). Data are shown as mean ± standard error of the mean (SEM) (n= 6 for vehicle, n=11 for seralutinib). Statistical analysis was performed using unpaired t-test. **P<0.005, ***P<0.001 versus vehicle.
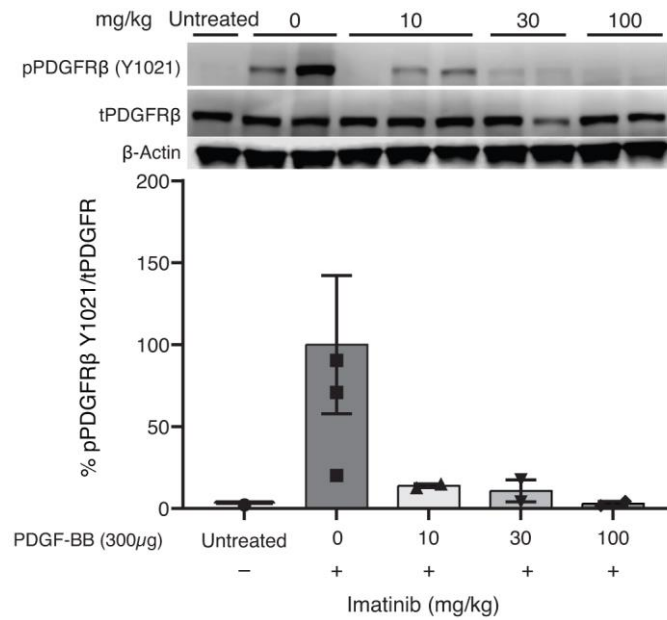
Figure S3. Imatinib in vivo pharmacodynamic (PD) profile. Male SD rats received vehicle (0 mg/kg) or imatinib 10mg/kg, 30mg/kg or 100mg/kg via oral gavage for two consecutive days. Rats were administered PDGF-BB via intratracheal insufflation into the lungs six hours post dose. Five minutes post-challenge, lungs were harvested to measure phosphorylation of PDGFR. Data presented as percent change in phospho PDGFRβ (Y1021)/ total PDGFRβ by western blot analysis. Data presented as mean ± SEM (n=1 for Naïve, n=4 for Vehicle, n=2 for all imatinib doses).
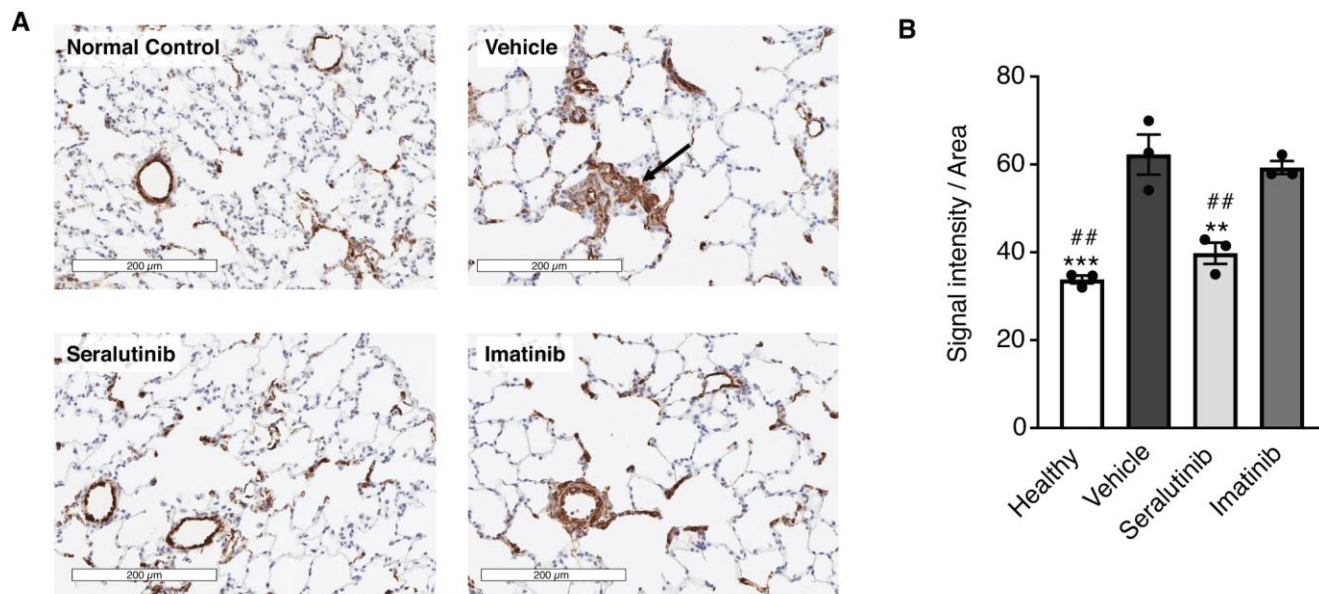
Figure S4. *(A)* Immunohistology of smooth muscle actin to visualize muscularization of pulmonary arteries in SU5416/H study. Representative image from normal, vehicle, seralutinib and imatinib treated lungs are shown. Arrow points to plexiform lesion in vehicle group. (*B*) Bar graph showing quantification of SMA stain. Data represents mean ± SEM, n=3 for all groups. Statistical analysis was performed using one-way ANOVA with Dunnett's multiple comparisons test. ***P<0.0001; **p<0.01 versus vehicle; ##p<0.01 versus imatinib. Scale bar, 200μm.
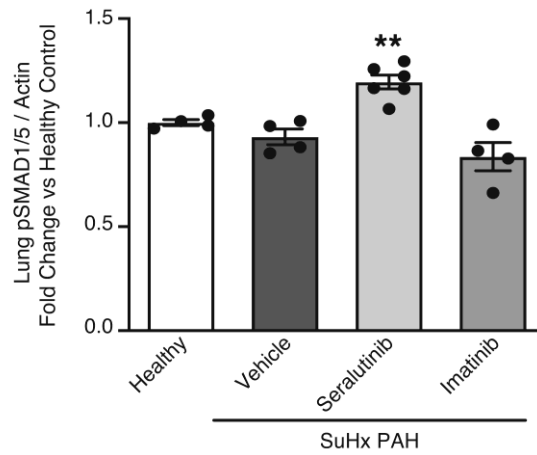
Figure S5. phospho-SMAD1/5 /β-Actin fold change in SU5416/H rat lungs relative to healthy controls at the end of the treatment period (day 49, Study 3). Data are presented as mean ± SEM (healthy (n=4), vehicle (n=4), seralutinib (n=6), imatinib (n=4)). Statistical analysis was performed using one-way ANOVA with Dunnett's multiple comparisons test, **P<0.005 versus vehicle.
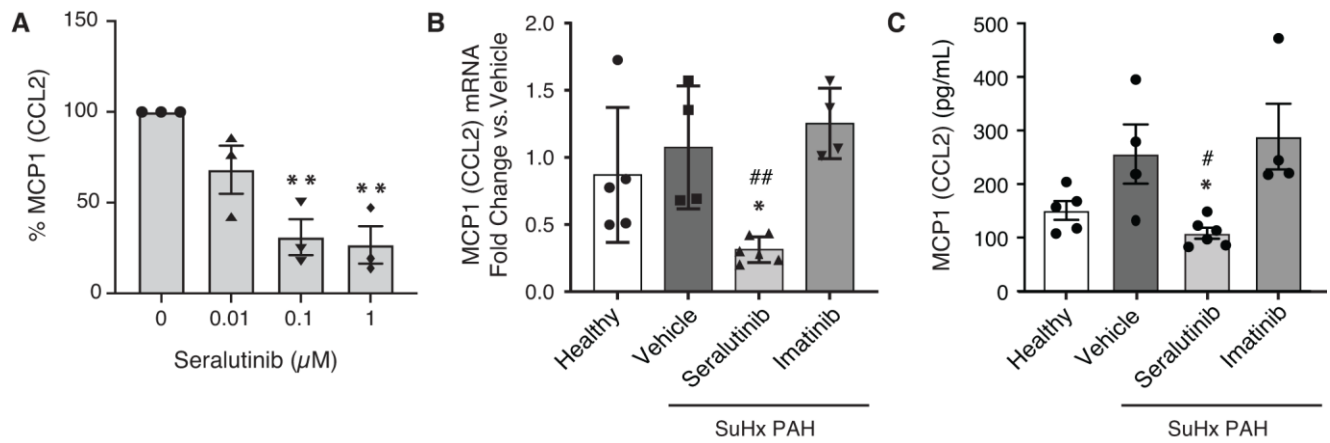
Figure S6. (*A*) Seralutinib effect on monocyte chemoattractant protein 1 (MCP-1/CCL2) secretion in primary human macrophages, determined after a 24-hour incubation with increasing concentrations of seralutinib. Data are shown as mean % expression relative to baseline ± SEM (n=3 independent donors). **$P<0.005$ versus vehicle. Impact of inhaled seralutinib or imatinib on monocyte chemoattractant protein 1 (MCP-1/CCL2) mRNA expression (B) or protein levels (*C*) in rat lungs from the SU5416/H pulmonary arterial hypertension (PAH) models at the end of treatment (day 49, Study 3). Data are shown as mean ± SEM (healthy (n=4), Vehicle (n=4), seralutinib (n=6) and imatinib (n=4)). Statistical analysis performed using one-way analysis of variance (ANOVA) with Dunnett's (mRNA) or Tukey's (protein) Multiple Comparisons Test. *$P<0.05$ versus vehicle, # $P<0.05$, ##$P<0.01$ versus imatinib.
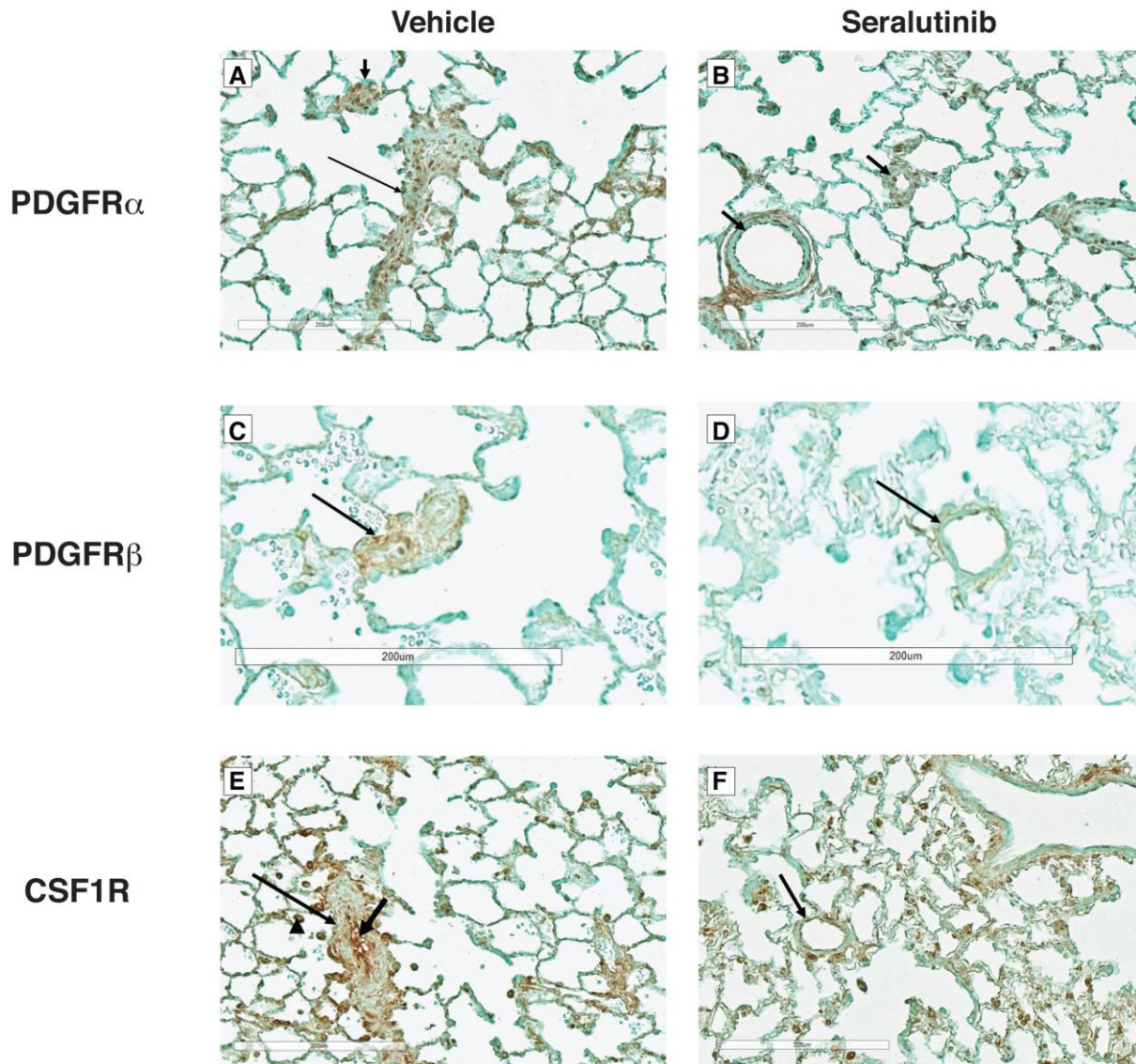
Figure S7. Representative lung tissue expression of PDGFRα (*A-B*), PDGFRβ (*C-D*) and CSF1R (*E-F*) in vehicle (*A, C, E*) and seralutinib (*B, D, F*) treated SU5416/H rats. (*A*) Lung from SU5416/H vehicle-treated rat stained for PDGFRα. Pulmonary arterial vessels are seen both in long axis (long arrow) and short axis (short arrow). High signal for PDGFRα is seen mostly in the media, but also in the neointima.

(*B*) Lung from SU5416/H seralutinib-treated rat showing patent small pulmonary arteries. PDGFRα is present but qualitatively decreased. Arrows point to small pulmonary arteries. (*C*) Lung from SU5416/H vehicle-treated rat stained for PDGFRβ. (*D*) Lung from SU5416/H seralutinib-treated rat stained for PDGFRβ. Arrows point to small pulmonary arteries. (*E*) Lung from SU5416/H vehicle-treated rat stained for CSF1R. Long arrow points to hypertrophied pulmonary artery. Short arrow points to neointima staining positive for CSF1R. Arrowhead points to an alveolar macrophage. (*F*) Lung from SU5416/H seralutinib-treated rat stained for CSF1R. Long arrow points to a small pulmonary artery.
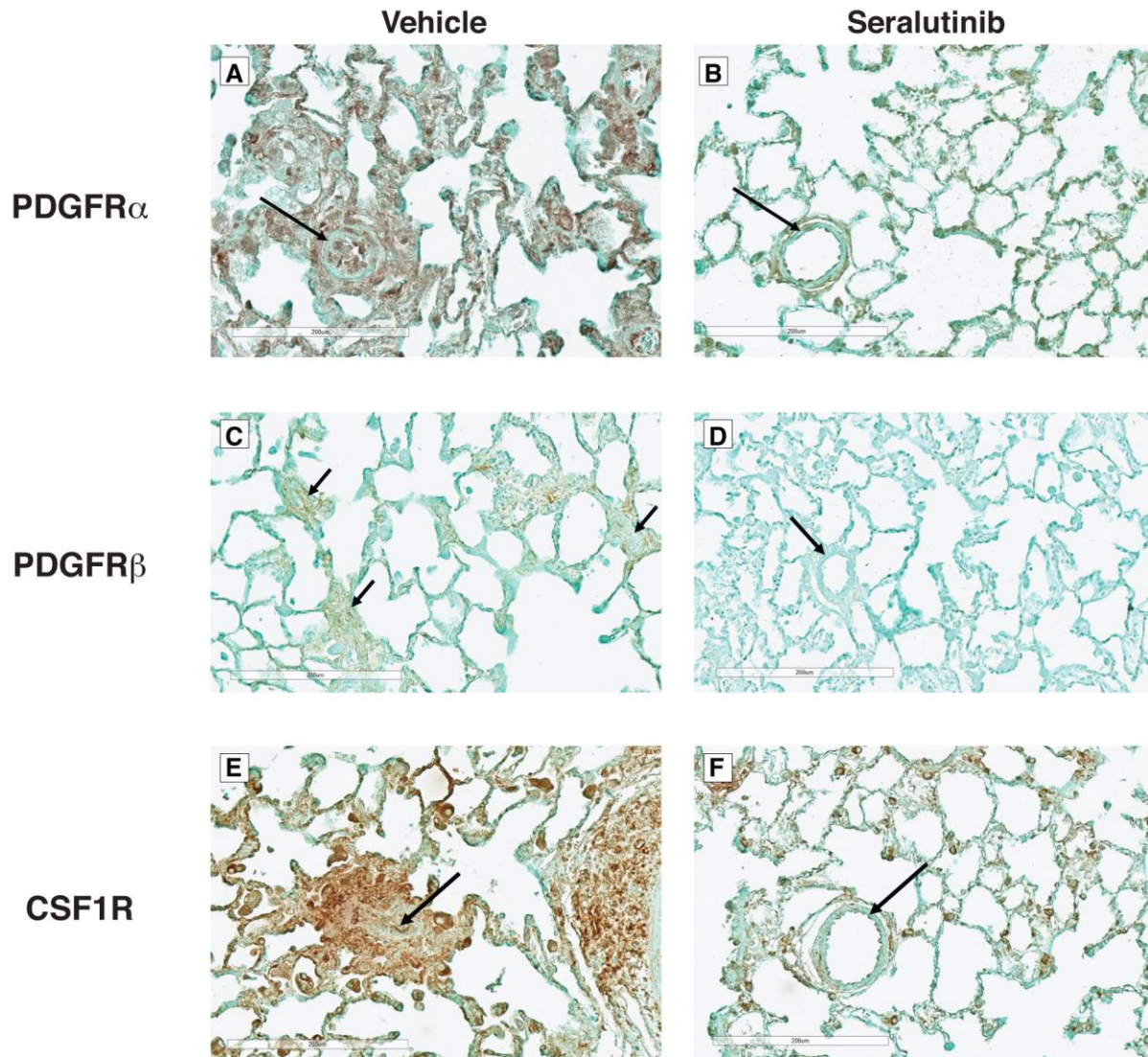
Figure S8. Representative lung tissue expression of PDGFRα (*A-B*), PDGFRβ (*C-D*) and CSF1R (*E-F*) in vehicle (A, C, E) and seralutinib (B, D, F) treated MCTPN rats. (*A*) Lung from MCTPN vehicle-treated rat stained for PDGFRα. High signal is noted in the neointima and perivascular area of small pulmonary arteries (arrow points to a small pulmonary artery. (*B*) Lung from MCTPN seralutinib-

treated rat stained for PDGFRα. Arrow points to a small pulmonary artery. (*C*) Lung from MCTPN vehicle-treated rat stained for PDGFRβ. Arrows point to small, essentially occluded, pulmonary arteries. Signal for PDGFRβ is distributed throughout the lesions. (*D*) Lung from MCTPN seralutinib-treated rat stained for PDGFRβ. Arrow points to a small pulmonary artery. There is very little signal for PDGFRβ. (*E*) Lung from MCTPN vehicle-treated rat stained for CSF1R. There is intense perivascular signal. Arrow points to occluded lumen of a small pulmonary artery. Arrowhead points to alveolar macrophage. (*F*) Lung from MCTPN seralutinib-treated rat stained for CSF1R. There is very little perivascular signal. Arrow points to small pulmonary artery.